bioRxiv preprint doi: https://doi.org/10.1101/676270; this version posted June 30, 2019. The copyright holder for this preprint (which was not certified by peer review) is the author/funder, who has granted bioRxiv a license to display the preprint in perpetuity. It is made available under aCC-BY-NC 4.0 International license.

Peroxiredoxin promotes longevity and H_2O_2-resistance in yeast through redox-modification of protein kinase A

Friederike Roger[1], Cecilia Picazo[1,2], Chikako Asami[1], Wolfgang Reiter[3], Sarah Hanzén[1], Chunxia Gao[1], Gilles Lagniel[4], Niek Welkenhuysen[5], Jean Labarre[4], Thomas Nyström[6], Morten Grøtli[1], Markus Hartl[3] and Mikael Molin*[1,2]

[1]Department of Chemistry and Molecular Biology, University of Gothenburg, SWEDEN

[2]Department of Biology and Biological Engineering, Chalmers University of Technology, Gothenburg, SWEDEN

[3]Mass Spectrometry Facility, Department of Biochemistry, Max F. Perutz Laboratories, University of Vienna, Vienna BioCenter, Vienna, AUSTRIA

[4]Oxidative Stress and Cancer Laboratory, Integrative Biology and Molecular Genetics Unit (SBIGEM), CEA Saclay, FRANCE

[5]Department of Mathematical Sciences, Chalmers University of Technology and University of Gothenburg, SWEDEN

[6]Department of Microbiology and Immunology, Institute for Biomedicine, Sahlgrenska Academy, University of Gothenburg

*Lead Contact for correspondence: mikael.molin@chalmers.se

Keywords

Aging, peroxiredoxin, H_2O_2 signaling, protein kinase A, glutathionylation, hormesis

bioRxiv preprint doi: https://doi.org/10.1101/676270; this version posted June 30, 2019. The copyright holder for this preprint (which was not certified by peer review) is the author/funder, who has granted bioRxiv a license to display the preprint in perpetuity. It is made available under aCC-BY-NC 4.0 International license.

Summary

Peroxiredoxins are modulators of aging in yeast and multicellular organisms. We have previously identified key roles for the peroxiredoxin Tsa1 in mechanisms by which caloric restriction boosts yeast H_2O_2 stress resistance and slows down replicative aging. The mechanisms by which peroxiredoxins stimulate H_2O_2 resistance and slow down aging are, however, still largely unclear. Here we show that the yeast peroxiredoxin Tsa1 boosts H_2O_2 resistance and slows down aging without affecting cellular H_2O_2 levels. Specifically, we pin-point a role of Tsa1 as an H_2O_2-receptor inhibiting nutrient signaling via protein kinase A (PKA) that governs both H_2O_2 resistance and longevity. Tsa1 controls PKA activity in a manner independent of the second messenger cAMP at the level of a conserved cysteine in the catalytic subunits. Stimulating Tpk1 redox-modification at this specific cysteine residue inhibits PKA activity and boosts cellular H_2O_2 resistance in part through dephosphorylating a conserved threonine in the kinase activation loop. Strikingly, preventing the phosphorylation of this threonine residue counteracts the H_2O_2 sensitivity of cells lacking Tsa1. These results are discussed in the context of an integrative model of aging where nutrient signaling pathways constitute hubs integrating information from multiple aging-related conduits and where the activity of a protein kinase can be fine-tuned by redox-modification through peroxiredoxins.

bioRxiv preprint doi: https://doi.org/10.1101/676270; this version posted June 30, 2019. The copyright holder for this preprint (which was not certified by peer review) is the author/funder, who has granted bioRxiv a license to display the preprint in perpetuity. It is made available under aCC-BY-NC 4.0 International license.

Introduction

Aging is a complex process affecting an organism on a molecular, cellular and tissue level . Many cellular processes affect the rate of aging and a number of so called gerontogenes, i.e. genes that extend lifespan when mutated, have been identified in model organisms [2]. Caloric restriction (CR) is an intervention that slows down aging and reduces the incidence of age-related disease in most organisms where it has been studied, from the unicellular organism baker's yeast [3] to rhesus monkeys [4]. Because of its near universal conservation there is considerable interest in understanding the downstream mechanisms by which this intervention reduces the rate of age-related decline and it is thought that elucidating such pathways will reveal key molecular mechanisms of aging.

It is clear from a number of studies that reduced nutrient signaling via insulin/insulin-like growth factor (IGF-1), target-of-rapamycin and/or protein kinase A pathways is intimately linked to lifespan extension [5-8]. Reduced nutrient signaling promotes slower growth, insulin sensitivity and a general increase in stress resistance which is thought to lead to maintained health and a longer lifespan. More specifically, CR has been proposed to extend lifespan by increasing oxidative stress resistance thereby lowering cellular oxidative damage [9-12].

Recently, peroxiredoxins have emerged as conserved modulators of aging based on their requirement for the lifespan promoting effects of caloric restriction and CR-mimetic mutations/interventions [11, 13, 14]. 2-Cys peroxiredoxins (Prx) are obligate dimers carrying two cysteines, one of which reduces H_2O_2 (Cys48 in yeast Tsa1), thereby forming a sulfenic acid (Cys48-SOH). The other cysteine, in the second Prx molecule in the dimer (Cys171 in yeast Tsa1), resolves the Cys48-SOH by condensation into an inter-subunit disulfide between the two Tsa1 subunits in the dimer. The homodimer is resolved by thioredoxin leading to the accumulation of oxidized thioredoxin. In addition, Cys48-SOH can react further with H_2O_2, to form a sulfinic acid (Cys48-SOOH) which inactivates the catalytic cycle, while promoting multimerisation and a functional switch into a molecular chaperone [15, 16].

Notably, we found that CR increased both the H_2O_2 resistance and the lifespan of yeast cells by stimulating the activity of the most highly expressed of the typical 2-Cys peroxiredoxins, Tsa1 [11]. Similarly, the CR-mimetic drug metformin stimulates the activity of the Prdx-2 peroxiredoxin in worms in a manner extending lifespan [14]. Furthermore, neuronal peroxiredoxin overexpression was shown to extend lifespan in flies in the absence of caloric restriction [17] and so did mild overexpression of Tsa1 in yeast [18]. Conversely, peroxiredoxin-deficient mice, flies, worms and yeast all age prematurely [11, 17, 19, 20], intimately linking the activity of peroxiredoxins to molecular processes underlying aging.

Peroxiredoxins are known to be required for the maintenance of genome stability in several organisms [5, 6] and PrxI-deficient mice prematurely accumulate age-related tumors [19], suggesting a link to the prevention of a group of prevalent age-related diseases. Interestingly, we recently showed that Tsa1 reduced the amount of damaged/misfolded proteins accumulating in aged yeast cells [18], suggesting an importance in the prevention of aging factors linked also to other age-related diseases e.g. neurodegeneration [21].

Despite this, less is known about the exact mechanisms by which peroxiredoxins reduce the rate of aging. Neither the rate at which mutations accumulated in aging yeast cells nor H_2O_2 scavenging appear to be linked to the anti-aging effects since neither of them are altered in cells expressing a single extra copy of the *TSA1* gene which robustly extends lifespan (by 40%) [18]. We noted an increase in sulfinylated Tsa1 with age in yeast [11] pointing to the importance of this modification upon aging, possibly by promoting multimerization and chaperone activity [16]. In line with a role of

bioRxiv preprint doi: https://doi.org/10.1101/676270; this version posted June 30, 2019. The copyright holder for this preprint (which was not certified by peer review) is the author/funder, who has granted bioRxiv a license to display the preprint in perpetuity. It is made available under aCC-BY-NC 4.0 International license.

sulfinylated Tsa1 in counteracting age-related protein damage, we found Tsa1 sulfinylation crucial for guiding Hsp70/104 molecular chaperones to proteins aggregating upon increased age and H_2O_2 [18].

Notwithstanding the apparent prominent role of Tsa1 chaperone function, increased H_2O_2 resistance upon CR requires both Cys 48 and Cys 171 [11] and Prdx-2 dimers accumulated upon metformin treatment in worms [14] suggesting that some of the beneficial effects of CR and CR-mimetic interventions are linked to peroxiredoxin catalytic cycling. Hydrogen peroxide can work as a signaling molecule and peroxiredoxins are able to transfer the signal to target proteins by reversibly oxidizing cysteine residues [22, 23]. We recently showed that, in response to H_2O_2, Tsa1 and thioredoxin were required to inhibit PKA-mediated repression of the transcription factor Msn2 leading to its activation . This is interesting since CR previously has been shown to extend lifespan by reducing PKA kinase signaling [3, 11]. In worms, increased Prdx-2 function upon metformin treatment was connected to increased PMK-1/p38 mitogen-activated protein kinase (MAPK) activity [14] further pointing to a link of signaling via both catalytic cysteines of 2-Cys peroxiredoxins to stress-responsive kinases.

Here we show that the hydrogen peroxide sensitivity and premature aging seen in cells lacking Tsa1 is not related to defective H_2O_2 scavenging but rather to aberrant nutrient signaling through protein kinase A (PKA). Tsa1 interacts both genetically and physically with PKA at the level of the catalytic subunits. We identified Tsa1-dependent redox-modification of the most highly expressed PKA catalytic subunit targeting a conserved cysteine that is specifically required for Tsa1-mediated H_2O_2 resistance. Redox-modification reduced enzyme activity and increased H_2O_2 resistance in part through dephosphorylating a conserved threonine (Thr241) in the kinase activation loop and, remarkably, preventing Thr241 phosphorylation restored H_2O_2 resistance to Tsa1-deficient cells. These results indicate that peroxiredoxins slow down the rate of aging through a unique role in kinase signaling and suggest a novel mode of regulation of the conserved nutrient-sensing cascade PKA impinging on aging.

bioRxiv preprint doi: https://doi.org/10.1101/676270; this version posted June 30, 2019. The copyright holder for this preprint (which was not certified by peer review) is the author/funder, who has granted bioRxiv a license to display the preprint in perpetuity. It is made available under aCC-BY-NC 4.0 International license.

Results

Tsa1 slows down aging in a manner dependent on both catalytic cysteines but independent on H_2O_2 scavenging

To clarify the mechanism by which Tsa1 promotes longevity we analyzed the lifespans of *tsa1C48S* (Cys48Ser) and *tsa1C171S* (Cys171Ser) mutants (Fig. 1A). We analyzed the lifespans both of mutants created by replacing the wild-type gene and in strains lacking genomic *TSA1* but expressing mutant *tsa1* from a plasmid (Fig. S1). In agreement with a crucial role of the catalytic cysteines in lifespan control *tsa1C48S* and *tsa1C171S* cells suffered a lifespan as short as cells lacking Tsa1 altogether. In addition, cells expressing a truncated form of Tsa1 lacking the C-terminal YF motif (*tsa1ΔYF*), which is less sensitive to hyperoxidation [18], had a near wild-type lifespan, supporting the idea that both Tsa1 catalytic cysteines and only to a minor extent Tsa1C48 hyperoxidation are important for peroxiredoxin-mediated control of the rate of aging.

We next inquired whether the H_2O_2-sensitivity and short lifespan of cells lacking Tsa1 was caused by defective H_2O_2-scavenging. In a first assay we exposed cells to H_2O_2 and monitored its decay in the extracellular milieu. Like cells expressing an extra copy of *TSA1* [18], Tsa1-deficient cells reduced exogenous H_2O_2 as efficiently as did wild-type cells (Fig. 1B). To measure H_2O_2 levels in cells lacking Tsa1 specifically in the context of aging we expressed the genetically encoded H_2O_2 sensor HyPer3 in aged cells. Upon H_2O_2 addition this ratiometric sensor shows a C199-dependent increase in fluorescence at 500 nm, whereas the fluorescence at 420 nm is reduced [25] resulting in a dramatic increase in the fluorescence ratio 500 nm/420 nm, Fig. 1C). In wild-type cells of about 10 generations of age we observed a modest but significant increase in the H_2O_2 specific 500 nm/420 nm fluorescence ratio compared to young control cells. Tsa1-deficient cells suffered a similar or lower increase in the H_2O_2-specific fluorescence ratio as the wild-type. In cells expressing an extra copy of the *TSA1* gene, that exhibit an about 40% extended lifespan compared to control cells [18], the H_2O_2-specific HyPer3 signal increased to a similar or increased extent in aged cells (Fig. 1D). We conclude that the importance of both Tsa1 cysteines in aging control cannot be attributed to a role in H_2O_2 scavenging.

Increased H_2O_2 sensitivity and premature aging in cells lacking Tsa1 can be counteracted by Rasdeficiency

Tsa1 decreases PKA-dependent phosphorylation of the transcription factor Msn2 [24] and PKA has been shown to antagonize both longevity [3] and cellular H_2O_2-defences [11]. Therefore, we next evaluated to what extent PKA activity contributed to the short lifespan and H_2O_2-sensitivity of Tsa1-deficient cells. To accomplish this we combined Tsa1 deletion with Ras2 deficiency, which largely abrogates PKA stimulation by glucose and keeps PKA-activity at low levels still compatible with growth (Fig. 2A,). We previously noted that mid-exponential phase cultures (OD 0.5, [11]) acquire H_2O_2 resistance as a result of reduced PKA activity. We thus assayed H_2O_2-resistance of cells lacking Tsa1 and Ras2 both in early and mid-exponential phase. Interestingly, Ras2 deficiency completely counteracted the reduced lifespan (Fig. 2B) and H_2O_2-sensitivity (Fig. 2C) of cells lacking Tsa1, in early as well as mid-exponential growth phase, suggesting that these phenotypes of cells lacking Tsa1 were caused by aberrantly increased PKA activity. In support for this, suppression did not appear to involve increased H_2O_2 scavenging (Fig. S2A). Potentially pertaining to the mechanism of suppression, the expression of both the peroxiredoxins Tsa2 [27] and Dot5 were previously shown to increase as a result of decreased PKA activity. However, Ras2 deficiency was able to partly overcome also the H_2O_2-sensitivity of cells lacking both cytosolic thioredoxins (Fig. S2B), indicating peroxiredoxin-independent suppression, since peroxiredoxins depend on thioredoxin for reducing

bioRxiv preprint doi: https://doi.org/10.1101/676270; this version posted June 30, 2019. The copyright holder for this preprint (which was not certified by peer review) is the author/funder, who has granted bioRxiv a license to display the preprint in perpetuity. It is made available under aCC-BY-NC 4.0 International license.

power to remove H_2O_2 [5, 6]. Ras2 has been suggested to control aging also by a PKA-independent pathway potentially suggesting that Tsa1-dependent aging-control might involve a pathway different than PKA. To assay whether the suppression of the short lifespan and H_2O_2-sensitivity in Tsa1-deficient cells conferred by Ras2-deficiency was linked to reduced PKA activity, we deleted the high affinity cAMP-phosphodiesterase *PDE2* in cells lacking Ras2 and Tsa1 to again increase PKA activity. *PDE2* deletion restored both the H_2O_2-sensitivity (Fig. S2C) and the accelerated aging of Tsa1-deficient cells, despite that these cells also lacked *RAS2* (Fig. 2D). Furthermore, Pde2 deficiency and Tsa1-deficiency appeared to impinge on the same pathway of aging-control since cells lacking either of the proteins were as short-lived and H_2O_2-sensitive as cells lacking both (Fig. 2D, Fig. S2C). Like Ras2-deficiency, overproduction of the Ras-GTPase activating protein (GAP) Ira2, which reduces the levels of active Ras (Ras-GTP, see below) was also able to overcome H_2O_2 sensitivity of cells lacking Tsa1 (Fig. 2E) in a manner dependent on decreased PKA activity, since *pde2Δtsa1Δ* cells overproducing Ira2 were sensitive to H_2O_2 (Fig. 2E).

We conclude that H_2O_2-sensitivity and the short lifespan of cells lacking Tsa1 is linked to aberrantly increased PKA activity.

Tsa1 catalytic cycling slows down growth in Ras-deficient cells

Cells lacking Ras2 grew significantly slower than the wild-type (Fig. 3A, Fig. S2C) consistent with substantial inhibition of PKA. In contrast, cells lacking both Ras2 and Tsa1 grew at a rate indistinguishable from Tsa1-deficient cells (Fig. 3A), in support of that Tsa1 inhibits PKA activity. To substantiate this apparent contribution of Tsa1 to PKA-dependent growth control, we overexpressed the RasGTPase-activating protein Ira2, which decreases Ras activity [, see below] thereby decreasing growth to only approximately half the rate of control cells (Fig. 3B-C). The slow growth of cells overproducing Ira2 appeared to be caused by insufficient Ras-GTP levels (see below) and reduced PKA activity (Fig. 3D), since expression of the RasGTPase-activating protein-resistant *RAS2G19V* allele [[30], Fig. S3A-B] or abrogated cAMP degradation, due to lack of the cAMP phosphodiesterase Pde2 brought back growth to wild-type rates (Fig. 3C). Strikingly, Tsa1-deficiency restored the slow growth of cells overproducing Ira2 to the level of vector control cells (Fig. 3B-C). Suppression of the slow growth in Ras-deficient cells appeared to involve increased PKA activity, since the expression of Msn2/4 target genes decreased upon Tsa1-deficiency (Fig. 3D, Fig. S3C). Moreover, restored growth required increased PKA activity since the overproduction of both Pde2 and Ira2 in cells lacking Tsa1 again slowed down growth to the rates of wild-type cells overproducing Ira2 (Fig. 3E-F).

To investigate the mechanism by which Tsa1 inhibits PKA upon Ras deficiency, we overproduced Ira2 in Tsa1-mutants carrying serine substitutions of the catalytic cysteines C48 and C171 or in cells expressing a truncated Tsa1 lacking the C-terminal YF-motif required for hyperoxidation (*tsa1ΔYF*, [24]). Strikingly, *tsa1C171S* substitution suppressed the slow growth of Ira2 overproducing cells (Fig. 3B-C) and reduced the expression of *CTT1* and *HSP12* (Fig. 3D), whereas slow growth and high *CTT1*/*HSP12* mRNA levels were maintained in *tsa1ΔYF* cells (Fig. 3B-D), indicating that both Tsa1 catalytic cysteines are involved in PKA repression. We previously observed that Tsa1-mediated H_2O_2-signaling to PKA requires thioredoxin [24] and we suggested that this proceeded by Tsa1 transducing the H_2O_2 signal through oxidizing the thioredoxins. In analogy with this, slow growth (Fig. 3B-C) and the increased expression of Msn2/4 targets (Fig. S3C) upon Ras-deficiency was absolutely dependent on the presence of cytosolic thioredoxins (Trx1 and Trx2).

Taken together, the data suggest that in Ras-deficient cells both Tsa1 catalytic cysteines restrain PKA-dependent phosphorylation through a mechanism involving the thioredoxins.

bioRxiv preprint doi: https://doi.org/10.1101/676270; this version posted June 30, 2019. The copyright holder for this preprint (which was not certified by peer review) is the author/funder, who has granted bioRxiv a license to display the preprint in perpetuity. It is made available under aCC-BY-NC 4.0 International license.

A single extra copy of *TSA1* slows down aging by mildly reducing PKA activity

We previously observed that a single extra-copy of the *TSA1* gene substantially extended lifespan in the absence of caloric restriction [18] and we sought to elucidate to what extent this modest increase in Tsa1 levels had an impact on PKA signaling. Interestingly, cells mildly overexpressing Tsa1 displayed increased accumulation of the reserve carbohydrate glycogen (Fig. 4A). In addition, they displayed increased expression of the sensitive PKA and Msn2/4 target Hsp12 (Fig. 4B) and were resistant to H_2O_2 (Fig. 4c), effects of an extra copy of the *TSA1* gene that were dependent on reduced PKA activity since they were lost in cells lacking Pde2 (Fig. 4B-C). The translation of the *SRX1* gene is more efficient following H_2O_2 addition in cells exhibiting reduced PKA-activity resulting in Tsa1 returning more quickly to the catalytic cycle [11]. In further support for *TSA1* merodiploid cells expressing reduced PKA activity, the fraction of hyperoxidized Tsa1 was reduced in such cells 30 minutes following the addition of 0.6 mM H_2O_2 (Fig. S4A). This effect was dependent on *SRX1* and on reduced PKA activity, since Srx1- or Pde2-deficiencies made Tsa1 sensitive to hyperoxidation irrespective of *TSA1* copy number.

Next, we assayed the lifespans of wild-type and Pde2-deficient cells expressing one or two *TSA1* copies (Fig. 4D). In agreement with a crucial role of PKA inhibition for a single extra copy of *TSA1* to slow down the rate of aging, lifespan extension by moderately increased Tsa1 levels was substantially reduced in *pde2Δ* cells (6.7 ± 1%, longer lifespan in *pde2Δ* o/e *TSA1* versus *pde2Δ* control cells, n=3).

Whereas mutations that mildly reduce PKA activity have been noted to decrease the rate of aging (e.g. *cdc25-10*, *cdc35-1* [11, 31, 32], cells lacking the PKA catalytic subunits altogether completely arrest growth [33, 34], see below). Mutations more substantially inhibiting PKA activity without fatally compromising the ability to grow fall in between these two extremes (e.g. *ras2Δ* and *cdc25-1*, Fig. 2B, Fig. S4B). Mildly reduced PKA activity is thus expected to extend lifespan, whereas in mutants with more strongly inhibited PKA activity this beneficial effect on lifespan is lost and depending on the allele a near wild-type or a negative effect on lifespan is apparent. In support for an extra copy of *TSA1* only mildly inhibiting PKA activity, Hsp12 expression was induced to lower levels upon Tsa1 overproduction (Fig. 4B) than upon *RAS2* deletion (Fig. S3C).

Tsa1 affects PKA activity independent of active Ras and cAMP

To understand at what level in the pathway Tsa1 affects PKA activity, we measured the levels of PKA signaling intermediates in cells overproducing Ira2 in the presence and absence of Tsa1. As expected, overexpression of *IRA2* dramatically reduced the levels of active Ras (Ras-GTP) and this reduction was largely maintained in *pde2Δ* cells (Fig. 5A), in which PKA signaling is increased downstream of Ras. Consistent with a role also of Tsa1 in modulating PKA activity downstream of Ras, Tsa1-deficient cells overproducing Ira2 similarly exhibited very low Ras-GTP levels (Fig. 5A). Tsa1 appears to act downstream also of cAMP, since the levels of this intermediate were largely unaffected in cells lacking Tsa1, both upon normal and increased Ira2 levels (Fig. 5B). As expected, Pde2-deficiency increased cAMP levels independent of Ira2 levels (Fig. 5B), thus explaining restored growth in Pde2-deficient cells overproducing Ira2. Interestingly, the dramatic decrease in Ras-GTP seen upon Ira2 overproduction was only partly reflected in decreased cAMP, in agreement with the idea that PKA activity can be controlled also independent of cAMP [35].

Several of the regulatory proteins that act downstream of Ras, including the PKA negative regulatory subunit Bcy1, the high-affinity cAMP phosphodiesterase Pde2 or the downstream kinase Yak1 were identified in screens looking for mutants that suppress the lethality of *ras1Δras2Δ* double mutants [26,

bioRxiv preprint doi: https://doi.org/10.1101/676270; this version posted June 30, 2019. The copyright holder for this preprint (which was not certified by peer review) is the author/funder, who has granted bioRxiv a license to display the preprint in perpetuity. It is made available under aCC-BY-NC 4.0 International license.

33, 36]. These mutants are thought to bypass the requirement for Ras either by activating PKA independent of Ras (Bcy1 and Pde2) or by reducing the activity of downstream effectors, e.g. the kinase Yak1. In addition, loss of the PKA-controlled transcription factor Msn2 or both Msn2 and its homologue Msn4, can partially overcome the requirement for a PKA catalytic subunit-encoding (*TPK*)-gene [37] or sufficient levels of active Ras for cells to grow (Fig. 3C). We thus sporulated heterozygous *ras1Δ/RAS1*, *ras2Δ/RAS2* and *tsa1Δ/TSA1* diploid cells to learn whether the absence of Tsa1 similarly could compensate for the lack of Ras proteins. Among the wild-type and single mutant spores only the absence of *RAS2* conferred a moderately increased spore lethality (3 out of 18 spores or 17%, Fig. 5C) consistent with the significantly reduced PKA activity of such cells. The increased spore lethality in Ras2-deficient cells seemed to, in part, be mediated by Tsa1, since none of the 20 *ras2Δtsa1Δ* spores died, suggesting that Tsa1 affected also spore germination downstream of Ras. Importantly, however, lack of Tsa1 was unable to bypass the requirement for either Ras1 or Ras2 for spore germination, since no cells lacking both Ras1 and Ras2 were viable irrespective of the presence or absence of Tsa1 (Fig. 5C). Along similar lines, lack of Tsa1 counteracted the moderately increased spore lethality of cells lacking the *TPK2* and/or *TPK3* genes encoding PKA catalytic subunits (Fig. S5A), but could not overcome the requirement of a single PKA catalytic subunit for spore germination [34]. This since we were unable to obtain viable *tsa1Δ tpk1Δ tpk2Δ tpk3Δ* spores in a cross between haploid *tsa1Δ* and *tpk1Δ tpk2Δ tpk3Δ* strains unless a centromeric *TPK1* plasmid, used to keep the *tpk1Δ tpk2Δ tpk3Δ* strain alive, was also present (in 6 out of 6 viable spores with the genomic *tsa1Δ tpk1Δ tpk2Δ tpk3Δ* genotype, Fig. S5A).

Taken together the data indicate that Tsa1 affects PKA downstream of the second messenger cAMP.

Tpk1 co-purifies with Tsa1 and significant proportion of Tpk1 molecules are glutathionylated on the conserved Cys243

Rat adipocyte type II PKA is inhibited by an H_2O_2-induced mixed disulfide between the regulatory and the catalytic subunit [38]. In addition, bovine and mouse PKA regulatory subunits dimerize through two intermolecular disulfide bonds in response to growth-factor and H_2O_2 [39]. We thus probed the redox-state of the regulatory subunit Bcy1 and of the most highly expressed of the catalytic subunits, Tpk1, in response to H_2O_2, in thioredoxin-deficient cells and in cells expressing *trx2C34S* 'cysteine-trap' mutant. Neither Bcy1 nor Tpk1 displayed redox-dependent altered mobility in response to H_2O_2 and in thioredoxin-deficient cells nor did they present significant amounts of mixed disulfides in a strain expressing the *TRX2* cysteine-trap mutant (Fig. S5B-C). Mixed Trx2 disulfides, however, accumulated in *trx2C34S* but not *trx2C31SC34S* cells, suggesting efficient trapping of Trx2-Cys31 targets (Fig. S5C, NR, lanes 5-6 and 10-11 [Trx2-ProtA]).

We noted that overproduction of the PKA regulatory subunit (mc-*BCY1*) could not overcome the PKA signaling defect in Tsa1-deficient cells despite increasing the Msn2 response dramatically in Tsa1 proficient cells (Fig. 5D). In addition, the cysteine in the rat type II PKA regulatory subunit engaged in an intermolecular disulfide bond bridging the regulatory and the catalytic subunits, is only conserved in vertebrates and not in yeast [[38], see also below Fig. S6A-B].

Therefore, we next focused our attention on the catalytic subunits. In order to in an unbiased manner search for post-translational modifications and covalent interactors of Tpk1 we undertook liquid chromatography mass spectrometric analysis of tagged, affinity-purified His- and biotin-tagged Tpk1 (Tpk1-HB,). In an initial database search we focused on a set of known plausible PTMs, such as oxidation, sulfinylation and glutathionylation of cysteines in addition to the phosphorylation of serine, threonine and tyrosine residues. We also utilized an unbiased open search approach to identify further

bioRxiv preprint doi: https://doi.org/10.1101/676270; this version posted June 30, 2019. The copyright holder for this preprint (which was not certified by peer review) is the author/funder, who has granted bioRxiv a license to display the preprint in perpetuity. It is made available under aCC-BY-NC 4.0 International license.

unknown modifications, which revealed further yet undefined PTMs of Tpk1 (Supplemental Table S1, Fig. S5D-E). Based on these results we selected set of peptides covering the most abundant PTMs of Tpk1 and performed a quantitative analysis employing label free quantification of MS1 peaks, followed up by a targeted MS/MS approach applying parallel reaction monitoring (PRM), to determine quantitative changes in the PTM pattern upon H_2O_2 exposure.

Interestingly, we identified glutathionylated Tpk1Cys195 (Tpk1-Cys195-SSG, Fig. S5F, Supplementary data Table S2) and Cys243 (Cys243-SSG, Fig. 5E) peptides even in the absence of H_2O_2. Label-free quantification and PRM suggested that the levels of all three Cys195 peptides detected decreased dramatically (6 and 11-fold) upon the addition of 0.4 mM and 0.8 mM H_2O_2, respectively), suggesting that Cys195 engages in other unknown redox modifications under these conditions (Fig. S5f, Supplemental Tables S3 and S4).

Five different Cys243 modified peptides (C243-SH T241-P, C243-SSG T241-P, C243-SOOH T241-P, C243-SH T241, C243-SSG T241, Fig. 5F, Fig. S5G, Supplemental Table S2) were detected. The former three peptides were phosphorylated at Thr241. We noted that the PRM signals of glutathionylated and non-glutathionylated peptides were of the same magnitude, suggesting that a significant fraction of Tpk1 is glutathionylated in the absence of H_2O_2 (Fig. 5F, Supplementary Table S4). Upon H_2O_2 treatment the quantities of the peptide species Cys243-SH Thr241 and Cys243-SSG Thr241 only marginally increased (1.4-fold increased levels of both, Fig. 5F). However, open search results suggested the formation of Cys243-dependent redox modifications other than glutathionylation upon H_2O_2 addition, which are not covered in our quantitative MS analysis, but which could also be involved in Tpk1 inactivation (Fig. S5E). However, the quantities of neither of these modifications, as determined by label-free quantification, increased upon the addition of H_2O_2 (Supplemental Table S5).

Interestingly, however the levels of all three Thr241 phosphorylated peptide species (C243-SH T241-P, C243-SSG T241-P, C243-SOOH T241-P) decreased (2.4-, 2.4- and 3.2-fold, respectively, Fig. 5F, Fig. S5G). Notably, phosphorylated Thr241 stimulates PKA activity (see below), and therefore the decrease in these Thr241 phosphorylated peptides also supports PKA inactivation upon H_2O_2 addition.

In addition, database searches identified no less than 15 peptides matching Tsa1 in proteins co-purified with Tpk1-HB (Supplementary data Table S6) suggesting a direct role of Tsa1 in Tpk1 modification. The amount of Tsa1 decreased 2.4 and 2.7-fold following the addition of 0.4 mM and 0.8 mM H_2O_2, respectively (Fig. S5H, Supplemental Table S7). These results indicated a direct interaction between Tsa1 and Tpk1 that diminished upon H_2O_2 treatment.

To find support for the idea that redox modifications of Tpk1 increased upon H_2O_2 addition, we used the PEG-maleimide assay in which oxidized cysteines are alkylated by PEG-maleimide, whereas, reduced cysteines are alkylated by N-ethylmaleimide (NEM) adding 5 kDa of molecular weight per oxidized cysteine [41]. Interestingly, following immunoblot using a Tpk1-specific antibody, a Tpk1 band of slower migration, consistent with the addition of mPEG appeared already in unstressed cells [41]. The intensity of this band increased in mPEG treated extracts from *TPK1 tpk2Δ tpk3Δ* cells following H_2O_2 addition (Fig. 5G, mPEG panel), but not in extracts where both reduced and oxidized cysteines where alkylated with NEM (Fig. 5G, NEM panel). In support for the increased intensity of this band following H_2O_2 addition representing Tpk1C243 modification the intensity of this mPEG band did not increase in *tpk1C243A tpk2Δ tpk3Δ* mutant cells (Fig. S5I).

A Tpk1 homology models suggests that Cys243 glutathionylation decreases PKA activity similar to in mouse type II PKA *in vitro*

bioRxiv preprint doi: https://doi.org/10.1101/676270; this version posted June 30, 2019. The copyright holder for this preprint (which was not certified by peer review) is the author/funder, who has granted bioRxiv a license to display the preprint in perpetuity. It is made available under aCC-BY-NC 4.0 International license.

Glutathionylation of the cysteine homologous to Tpk1Cys243 in mouse type II catalytic subunit in PKA (Cys199) has previously been shown to reduce kinase activity *in vitro* [42]. This modification was proposed to destabilize the activation loop leading to the dephoshorylation of a conserved threonine (Thr197) in this motif, less efficient substrate interaction and reduced enzyme activity [42, 43]. In analogy to the *in vitro* studies performed on the mouse enzyme we found that Tpk1-Cys243 redox modification correlated with decreased levels of all three phosphorylated Tpk1-Thr241-peptides detected, and moderately increased levels of a non-phosphorylated Thr241 peptide (Fig. 5F).

To evaluate whether yeast Tpk1 could be redox-regulated by a mechanism similar to that proposed for the mouse enzyme *in vitro*, we built a structural homology model of Tpk1 based on the mouse enzyme (Fig. 6A-B). The overall architecture of the yeast and mouse PKA holoenzymes were highly similar although the yeast enzyme lacked a cysteine in the regulatory subunit through which the mouse and rat type II regulatory subunits may form a mixed disulfide with the catalytic subunit under oxidative conditions [Fig. S6A-B, [38]]. Analogous to in the mouse enzyme Thr241 phosphorylation stabilized the activation loop in the catalytic subunit of the yeast enzyme through hydrogen bonds to Arg209 and Lys233 (Fig. 6C). On the contrary, in the Thr241 non-phosphorylated state these hydrogen bonds were lacking leading to an overall distortion of the structure and Lys233 interaction with Glu130 and Asp134 (Fig. 6D). Docking experiments with glutathionylated Cys243 suggested that Cys243-SSG stabilized the Thr241 dephosphorylated state by direct hydrogen bonding (Fig. 6E). Upon Cys243 glutathionylation in the Thr241 phosphorylated enzyme the glutathione moiety adopted a different structure instead extending into the ATP binding pocket (Fig. 6F).

In summary, homology modelling suggested that glutathionylation of the conserved Cys243 residue inhibits PKA activity by destabilizing the activation loop of the enzyme and/or by interfering with ATP binding. Together with the quantitative MS data above these results suggest that a significant proportion of Tpk1 molecules are inactive in unstressed cells.

Tpk1 Cys243 glutathionylation and dephosphorylation of the activation loop of PKA increases H_2O_2 resistance

To assess the physiological impact of the conserved cysteine 243 of the Tpk1 catalytic subunit we substituted this cysteine with alanine in cells expressing *TPK1* as the only catalytic subunit (*tpk2Δtpk3Δ*) and assessed PKA related phenotypes. Whereas Tpk2 and Tpk3 deficient cells grew at a rate only marginally slower than the wild-type (Fig. 6G, Fig. S6C), counterselecting *TPK1* in these cells resulted in a complete inability to grow (Fig. S6D-E). In contrast, the cysteine-substituted *tpk1C243A* allele supported normal growth (Fig. S6C-E). We therefore next assessed the H_2O_2 resistance of these cells (Fig. 6G). Interestingly, whereas cells lacking Tpk2 and Tpk3 were marginally more resistant to H_2O_2 than wild-type cells, *tpk1C243A* mutant cells were sensitive to H_2O_2, suggesting that Tpk1 cysteine 243 is required to repress PKA activity and to sustain a normal ability to resist H_2O_2. Oxidation of cysteine residues, to e.g. sulfenic and sulfinic acids, may be mimicked by substitution into a charged amino acid, e.g. aspartate. We found that H_2O_2 resistance and other PKA related phenotypes of cells expressing *tpk1C243D* as the sole PKA catalytic subunit were indistinguishable from *TPK1* expressing isogenic strains (Fig. S6C-F) indicating that bulkier Tpk1C243 redox-modifications may be required to reduce PKA activity upon H_2O_2 stress. This view is supported by molecular dynamics simulations using a Tpk1 homology model, in which Cys243 was replaced with Asp. In contrast to glutathionylation of Cys243, the Asp modification only resulted in minor structural changes in Tpk1 (Fig. S6G-H). In a similar manner, Cys243 methylthiolation (Cys-S-CH_3) that was one of the Cys243 modifications detected in unstressed cells (Fig. S5E), did not appear bulky enough to significantly affect the Tpk1 structure (Fig. S6G-H).

bioRxiv preprint doi: https://doi.org/10.1101/676270; this version posted June 30, 2019. The copyright holder for this preprint (which was not certified by peer review) is the author/funder, who has granted bioRxiv a license to display the preprint in perpetuity. It is made available under aCC-BY-NC 4.0 International license.

Since MS data showed a decreased abundance of peptides phosphorylated at Thr241 in the activation loop of Tpk1 upon the addition of H_2O_2, we assayed the phenotypes of *tpk1T241A* mutation in otherwise Tpk2 and Tpk3-lacking cells. Whereas *tpk1T241A* mutant cells grew at normal rates (Fig. S6D-F) they were resistant to H_2O_2 (Fig. 6G), in keeping with the idea that reduced phosphorylation of Thr241 moderately decreases PKA activity and makes cells resistant to H_2O_2.

Tsa1-mediated H_2O_2 resistance requires Tpk1C243 and the destabilization of the Tpk1 activation loop

We next sought to evaluate whether Tsa1 influenced Tpk1 glutathionylation. Therefore we immunoprecipitated Tpk1-HB from Tsa1-proficient and –deficient cells and assayed glutathionylation by anti-glutathione immunoblot (Fig. 6H). Whereas Tpk1 glutathionylation seemed unaffected in the Tsa1-mutant in the absence of H_2O_2, the decreased Tpk1 glutathionylation seen in the wild-type was lost in cells lacking Tsa1, suggesting a key role of Tsa1 in governing Tpk1 redox status upon H_2O_2 addition.

To evaluate the importance of Tpk1C243 in Tsa1-mediated H_2O_2 resistance we assayed the H_2O_2 resistance of *TSA1/TSA1* merodiploid and *TSA1*/vector control cells expressing *TPK1* or *tpk1C243A* as the sole PKA catalytic subunit. Interestingly, in support for C243-dependent redox modification playing a crucial role in Tsa1-mediated H_2O_2 resistance Tpk1C243 appeared to be essential for the H_2O_2 resistance conferred by an extra copy of the *TSA1* gene (Fig. 6I).

Finally, we sought to evaluate whether dephosphorylation of the activation loop in the catalytic subunit of PKA contributed to Tsa1-dependent H_2O_2 resistance. To this end, we expressed the *tpk1T241A* allele as the sole catalytic subunit in cells lacking Tsa1 and assessed H_2O_2 resistance. In support for a crucial role for destabilization of the Tpk1 activation loop in Tsa1-mediated H_2O_2 resistance the *tpk1T241A* allele was able to overcome the H_2O_2 sensitivity of *tsa1Δ* cells (Fig. 6J).

We conclude that the dominant cytosolic yeast peroxiredoxin Tsa1 impacts on H_2O_2 resistance via a mechanism involving redox modulation of a conserved cysteine in and dephosphorylation of the activation loop in the catalytic subunit of protein kinase A.

bioRxiv preprint doi: https://doi.org/10.1101/676270; this version posted June 30, 2019. The copyright holder for this preprint (which was not certified by peer review) is the author/funder, who has granted bioRxiv a license to display the preprint in perpetuity. It is made available under aCC-BY-NC 4.0 International license.

Discussion

The ability of reduced caloric intake (caloric restriction) to extend the lifespan of organisms from yeast to primates has attracted much attention in the aging field. Since the incidence of many major age-related diseases such as cancer, diabetes and neurodegeneration is also reduced upon caloric restriction [4], there is hope that by reducing caloric intake or pharmaceutically targeting key molecular mechanisms underlying their beneficial health effects will fuel so called healthy ageing.

There is large consensus in the aging-field that reduced nutrient and/or growth signaling through less than a handful of conserved pathways (e.g. insulin/IGF-1, TOR and protein kinase A) is instrumental for caloric restriction to slow down aging. The contributions of the different pathways depends on the specific nutrient limitations imposed and on the organism [44]. Upon glucose restriction protein kinase A seems to play a key role [3, 45] and under such conditions the TOR kinase is regulated as a function of PKA in human cells [46]. In contrast, there is much more controversy regarding which downstream effector pathways/processes that are the most important in regulating the rate of aging. This could be a reflection of nutrient signaling coordinating the needs of many different cellular processes, the exact identity of which may differ slightly between different organisms and/or CR protocols [44]. The fact that several of the target processes proposed (eg vacuolar pH control and protein homeostasis) reciprocally have been suggested to feed-back control nutrient signaling in themselves [5, 47, 48] has caused further controversy regarding which mechanisms are most important in slowing down aging. A more modern integrative view on aging, however, posits that different pathways and/or organelles may be intricately interconnected into so called integrons . The idea that all biological systems are organized into integrons goes back to Francois Jacob in 1970. Interconnectivity allows the function of subsystems that fail to be compensated for by others, but also, conversely, that the failure of one subsystem can lead to the progressive decline of all systems through sequential collapse of homeostasis [49].

Peroxiredoxins have emerged as regulators of aging stimulating longevity in organisms from yeast to multicellulars such as worms, flies and mice. This is supported by observations that deletion of specific peroxiredoxin genes abolish the beneficial effects on longevity upon caloric restriction or CR-mimetic intervention [11, 13, 14] or conversely, that enforced peroxiredoxin expression extends lifespan in the absence of caloric restriction [17, 18]. The fact that peroxiredoxins are conserved in organisms from bacteria to humans and that they can be targeted pharmaceutically suggests that they may constitute promising target enzymes for the development of drugs against age-related diseases.

We have previously shown that peroxiredoxin activity is crucial for molecular chaperones to bind to aggregates forming in aged yeast cells [18], thus connecting peroxiredoxins to an aging factor conserved in many organisms. We linked this role in guiding molecular chaperones to proteins aggregating in aged cells to the sulfinylation of the primary catalytic cysteine and enzyme double decamerisation, thus providing an *in vivo* relevance for the chaperone activity observed *in vitro* of this peroxiredoxin form [15, 16]. However, we previously observed that H_2O_2 resistance in CR cells required both catalytic cysteines [11]. In addition, metformin was observed to lead to increased accumulation of disulfide-linked Prdx-2 in worms, raising the question of what the impact of peroxiredoxin catalytic cycling, or both the peroxidatic and resolving cysteines, on aging is. Data reported in this study support the requirement of both cysteines of Tsa1 in slowing down aging, thus reinforcing the correlation between peroxiredoxin-stimulated longevity and hydrogen peroxide resistance. Surprisingly, however, the importance of the two peroxiredoxin catalytic cysteines, in both aging and H_2O_2 resistance, did not seem to stem from a role in H_2O_2 scavenging, since neither medium H_2O_2 levels nor intracellular cytosolic H_2O_2 levels were altered in cells lacking Tsa1 (Fig. 1). Taken

bioRxiv preprint doi: https://doi.org/10.1101/676270; this version posted June 30, 2019. The copyright holder for this preprint (which was not certified by peer review) is the author/funder, who has granted bioRxiv a license to display the preprint in perpetuity. It is made available under aCC-BY-NC 4.0 International license.

together with the Tsa1-dependent increased lifespan in cells grown in the continuous presence of low levels of H_2O_2 , these data clearly demonstrate that the anti-aging effect of peroxiredoxins originates in H_2O_2 signaling.

Peroxiredoxins have been proposed to affect signaling in several ways e.g. 1) through the flood-gate model in which peroxiredoxin inactivation leads to a transient and (local) build-up of H_2O_2 that oxidizes other signaling proteins [51, 52], 2) as redox-relay signal transducers transferring regulatory disulfide bonds to signaling proteins [53] and 3) as proteins that multimerize and switch function upon hyperoxidation [54].

The redundancy of Tsa1 hyperoxidation and the requirement for both Tsa1 catalytic cysteines and the thioredoxins in PKA control suggests that the activity of protein kinase A is redox-regulated. Our genetic data, furthermore, clearly points to regulation of PKA by Tsa1 acting directly on the PKA catalytic subunits.

In this respect our data suggesting a direct Tsa1-Tpk1 physical interaction and a requirement for Cys243 in H_2O_2 resistance mediated by mild Tsa1 overexpression are highly interesting. Our data are consistent with a model in which a significant proportion of the PKA catalytic subunit molecules are glutathionylated *in vivo*. The decreased ability of *tpk1C243A* mutant cells to resist H_2O_2 may reflect enzyme hyperactivity and PKA signaling normally being restrained by glutathionylation. The homologous cysteine in murine type II PKA (Cys199) has previously been shown to be sensitive to modification by redox-reactive compounds *in vitro*, e.g. glutathionylation following oxidation by diamide and incubation in the presence of glutathione, resulting in enzyme inactivation [42, 55]. In addition, the homologous cysteine in type II rat PKA is involved in intersubunit disulfide bond formation with the regulatory subunit [38]. Intersubunit disulfide bond formation was shown to decrease PKA activity already at very low levels of H_2O_2 *in vitro* (1 μM) highlighting the importance of this conserved cysteine in the catalytic subunit in oxidative PKA regulation. However, our data suggest that redox-modification of the catalytic subunit cysteine, but not the intersubunit disulfide bond, is the primary and more conserved mechanism of oxidative PKA control. Furthermore, whereas intersubunit disulfide formation is expected to lock the enzyme in an inactive state our data indicate that destabilization of the substrate binding activation loop may represent a more subtle regulatory mechanism to fine-tune PKA activity upon H_2O_2 addition. A pressing question for the future will be to identify the specific peroxiredoxin-stimulated cysteine modification reducing PKA activity upon H_2O_2 addition.

Interestingly, other studies suggest that the activities of both protein kinase G and A are activated by H_2O_2 [39, 56]. Specifically, the I alpha isoform of protein kinase G in rat cells, PKGIalpha, formed an interprotein disulfide linking its two subunits in cells exposed to exogenous H_2O_2, which activated the enzyme [56], suggesting that the regulation of PKA/PKG by H_2O_2 involves the same conserved cysteine in the catalytic subunit but leads to opposite effects. In a similar fashion *in vitro* studies suggest that the energy-sensing kinase AMPK is activated upon glutathionylation [57]. Thus the impact of oxidants on protein kinases seems to be different for different kinases. Interestingly, the AMPK study identified glutathione-S-transferase to interact with AMPK both *in vitro* and in rat liver, suggesting a potential importance of this enzyme family in protein kinase regulation.

In summary data presented here and in a previous study [18] point to two different mechanisms by which peroxiredoxins counteract aging and age-related disease (Fig. 7), one involving catalytic cycling and the inhibition of nutrient-related kinase signaling (Fig. 7A-B). This mechanism appears to be critical for yeast to sustain normal longevity and is probably involved also in the ability of CR to slow

bioRxiv preprint doi: https://doi.org/10.1101/676270; this version posted June 30, 2019. The copyright holder for this preprint (which was not certified by peer review) is the author/funder, who has granted bioRxiv a license to display the preprint in perpetuity. It is made available under aCC-BY-NC 4.0 International license.

down yeast aging, since CR stimulated H_2O_2 resistance in a manner dependent on Tsa1 catalytic cycling [11]. Along the same lines, metformin-stimulated longevity in worms probably also involves increased Prdx-2 catalytic cycling [14]. The second mechanism by which peroxiredoxins may inhibit aging and age-related disease is by stimulating chaperone-dependent protein quality control to counteract the conserved aging factor protein aggregates [Fig. 7C, [18]]. In particular, we showed that Tsa1 sulfinylation was necessary to guide the molecular chaperones Hsp70 and Hsp104 to aggregates forming in aged and H_2O_2-treated cells. This anti-aging mechanism thus seems to be independent of the here described role in inhibiting nutrient signaling which instead appears to be linked to Tsa1 catalytic cycling. The requirement of both reduced PKA nutrient signaling (Pde2, this study) and normal protein quality control [e.g. cytosolic Hsp70 activity by Ssa1/2, [18]] for mild Tsa1 overproduction to extend lifespan support a requirement of both these mechanisms in the ability of enhanced peroxiredoxin levels to extend lifespan (Fig. 7C).

In the integrative view of aging, it can be assumed that a key role in the aging process is played by cellular components and/or pathways that assimilate information from different subsystems such as the above described nutrient signaling pathways, the latter which would constitute good candidates of acting as such integrators. Hence, the involvement of central nutrient signaling pathways in the mechanisms by which peroxiredoxins slow down aging is in agreement with this notion and suggest that also other anti-aging regimens may impact on nutrient signaling.

Acknowledgements

We gratefully acknowledge Michel B Toledano for valuable comments on the manuscript and Karin Voordeckers, Joseph Heitman and Robert J Deschenes for reagents. This work was supported by grants from the Swedish research Council VR, Cancerfonden, the Foundation Olle Engkvist byggmästare and Carl Tryggers stiftelse (all to MM).

Author contributions

Conceptualization M.M, F.R.; Methodology M.M., W.R., M.H., C.G., N.W., J.L.; Investigation F.R., C.P., M.M., C.A., S.H., G.L.; Writing – Original Draft M.M., F.R.; Writing – Review and Editing, M.M., F.R., T.N., W.R., M.G.; Funding Acquisition M.M., M.H., T.N., M.G.; Supervision, M.M., M.G.

Declaration of interests

The authors declare that they have no conflict of interest.

bioRxiv preprint doi: https://doi.org/10.1101/676270; this version posted June 30, 2019. The copyright holder for this preprint (which was not certified by peer review) is the author/funder, who has granted bioRxiv a license to display the preprint in perpetuity. It is made available under aCC-BY-NC 4.0 International license.

References

1. Lopez-Otin, C., Blasco, M.A., Partridge, L., Serrano, M., and Kroemer, G. (2013). The hallmarks of aging. Cell *153*, 1194-1217.
2. Rattan, S.I. (1995). Gerontogenes: real or virtual? FASEB J *9*, 284-286.
3. Lin, S.J., Defossez, P.A., and Guarente, L. (2000). Requirement of NAD and SIR2 for life-span extension by calorie restriction in Saccharomyces cerevisiae. Science *289*, 2126-2128.
4. Mattison, J.A., Colman, R.J., Beasley, T.M., Allison, D.B., Kemnitz, J.W., Roth, G.S., Ingram, D.K., Weindruch, R., de Cabo, R., and Anderson, R.M. (2017). Caloric restriction improves health and survival of rhesus monkeys. Nature communications *8*, 14063.
5. Molin, M., and Demir, A.B. (2014). Linking Peroxiredoxin and Vacuolar-ATPase Functions in Calorie Restriction-Mediated Life Span Extension. Int J Cell Biol *2014*, 12.
6. Nystrom, T., Yang, J., and Molin, M. (2012). Peroxiredoxins, gerontogenes linking aging to genome instability and cancer. Genes Dev *26*, 2001-2008.
7. Kenyon, C.J. (2010). The genetics of ageing. Nature *464*, 504-512.
8. Fontana, L., Partridge, L., and Longo, V.D. (2010). Dietary Restriction, Growth Factors and Aging: from yeast to humans. Science *328*, 321-326.
9. Fontan-Lozano, A., Lopez-Lluch, G., Delgado-Garcia, J.M., Navas, P., and Carrion, A.M. (2008). Molecular bases of caloric restriction regulation of neuronal synaptic plasticity. Mol Neurobiol *38*, 167-177.
10. Schulz, T.J., Zarse, K., Voigt, A., Urban, N., Birringer, M., and Ristow, M. (2007). Glucose restriction extends Caenorhabditis elegans life span by inducing mitochondrial respiration and increasing oxidative stress. Cell Metab *6*, 280-293.
11. Molin, M., Yang, J., Hanzen, S., Toledano, M.B., Labarre, J., and Nystrom, T. (2011). Life span extension and H_2O_2-resistance elicited by caloric restriction require the peroxiredoxin Tsa1 in *Saccharomyces cerevisiae*. Mol Cell *43*, 823-833.
12. Sohal, R.S., and Forster, M.J. (2014). Caloric restriction and the aging process: a critique. Free Radic Biol Med *73*, 366-382.
13. Olahova, M., and Veal, E.A. (2015). A peroxiredoxin, PRDX-2, is required for insulin secretion and insulin/IIS-dependent regulation of stress resistance and longevity. Aging Cell *14*, 558-568.
14. De Haes, W., Frooninckx, L., Van Assche, R., Smolders, A., Depuydt, G., Billen, J., Braeckman, B.P., Schoofs, L., and Temmerman, L. (2014). Metformin promotes lifespan through mitohormesis via the peroxiredoxin PRDX-2. Proc Natl Acad Sci U S A *111*, E2501-2509.
15. Jang, H.H., Lee, K.O., Chi, Y.H., Jung, B.G., Park, S.K., Park, J.H., Lee, J.R., Lee, S.S., Moon, J.C., Yun, J.W., et al. (2004). Two enzymes in one; two yeast peroxiredoxins display oxidative stress-dependent switching from a peroxidase to a molecular chaperone function. Cell *117*, 625-635.
16. Noichri, Y., Palais, G., Ruby, V., D'Autreaux, B., Delaunay-Moisan, A., Nystrom, T., Molin, M., and Toledano, M.B. (2015). In vivo parameters influencing 2-Cys Prx oligomerization: The role of enzyme sulfinylation. Redox biology *6*, 326-333.
17. Lee, K.S., Iijima-Ando, K., Iijima, K., Lee, W.J., Lee, J.H., Yu, K., and Lee, D.S. (2009). JNK/FOXO-mediated neuronal expression of fly homologue of peroxiredoxin II reduces oxidative stress and extends life span. J Biol Chem *284*, 29454-29461.
18. Hanzen, S., Vielfort, K., Yang, J., Roger, F., Andersson, V., Zamarbide-Fores, S., Andersson, R., Malm, L., Palais, G., Biteau, B., et al. (2016). Lifespan Control by Redox-Dependent Recruitment of Chaperones to Misfolded Proteins. Cell *166*, 140-151.
19. Neumann, C.A., Krause, D.S., Carman, C.V., Das, S., Dubey, D.P., Abraham, J.L., Bronson, R.T., Fujiwara, Y., Orkin, S.H., and Van Etten, R.A. (2003). Essential role for the peroxiredoxin Prdx1 in erythrocyte antioxidant defence and tumour suppression. Nature *424*, 561-565.
20. Olahova, M., Taylor, S.R., Khazaipoul, S., Wang, J., Morgan, B.A., Matsumoto, K., Blackwell, T.K., and Veal, E.A. (2008). A redox-sensitive peroxiredoxin that is important for longevity has

bioRxiv preprint doi: https://doi.org/10.1101/676270; this version posted June 30, 2019. The copyright holder for this preprint (which was not certified by peer review) is the author/funder, who has granted bioRxiv a license to display the preprint in perpetuity. It is made available under aCC-BY-NC 4.0 International license.

tissue- and stress-specific roles in stress resistance. Proc Natl Acad Sci U S A *105*, 19839-19844.

21. Hartl, F.U. (2017). Protein Misfolding Diseases. Annu Rev Biochem *86*, 21-26.
22. Leichert, L.I., and Dick, T.P. (2015). Incidence and physiological relevance of protein thiol switches. Biol Chem *396*, 389-399.
23. Stocker, S., Van Laer, K., Mijuskovic, A., and Dick, T.P. (2017). The Conundrum of Hydrogen Peroxide Signaling and the Emerging Role of Peroxiredoxins as Redox Relay Hubs. Antioxid Redox Signal.
24. Bodvard, K., Peeters, K., Roger, F., Romanov, N., Igbaria, A., Toledano, M.B., Reiter, W., Käll, M., and Molin, M. (2017). Light-sensing via hydrogen peroxide and a peroxiredoxin. Nature communications *8*, 14791.
25. Bilan, D.S., Pase, L., Joosen, L., Gorokhovatsky, A.Y., Ermakova, Y.G., Gadella, T.W.J., Grabher, C., Schultz, C., Lukyanov, S., and Belousov, V.V. (2013). HyPer-3: A Genetically Encoded H2O2 Probe with Improved Performance for Ratiometric and Fluorescence Lifetime Imaging. ACS Chem Biol *8*, 535-542.
26. Toda, T., Uno, I., Ishikawa, T., Powers, S., Kataoka, T., Broek, D., Cameron, S., Broach, J., Matsumoto, K., and Wigler, M. (1985). In yeast, RAS proteins are controlling elements of adenylate cyclase. Cell *40*, 27-36.
27. Hong, S.K., Cha, M.K., Choi, Y.S., Kim, W.C., and Kim, I.H. (2002). Msn2p/Msn4p act as a key transcriptional activator of yeast cytoplasmic thiol peroxidase II. J Biol Chem *277*, 12109-12117.
28. Cha, M.K., Choi, Y.S., Hong, S.K., Kim, W.C., No, K.T., and Kim, I.H. (2003). Nuclear thiol peroxidase as a functional alkyl-hydroperoxide reductase necessary for stationary phase growth of Saccharomyces cerevisiae. J Biol Chem *278*, 24636-24643.
29. Sun, J., Kale, S.P., Childress, A.M., Pinswasdi, C., and Jazwinski, S.M. (1994). Divergent roles of RAS1 and RAS2 in yeast longevity. J Biol Chem *269*, 18638-18645.
30. Tanaka, K., Lin, B.K., Wood, D.R., and Tamanoi, F. (1991). IRA2, an upstream negative regulator of RAS in yeast, is a RAS GTPase-activating protein. Proc Natl Acad Sci U S A *88*, 468-472.
31. Lin, S.J., Kaeberlein, M., Andalis, A.A., Sturtz, L.A., Defossez, P.A., Culotta, V.C., Fink, G.R., and Guarente, L. (2002). Calorie restriction extends Saccharomyces cerevisiae lifespan by increasing respiration. Nature *418*, 344-348.
32. Petitjean, A., Hilger, F., and Tatchell, K. (1990). Comparison of thermosensitive alleles of the CDC25 gene involved in the cAMP metabolism of Saccharomyces cerevisiae. Genetics *124*, 797-806.
33. Garrett, S., and Broach, J. (1989). Loss of Ras activity in Saccharomyces cerevisiae is suppressed by disruptions of a new kinase gene, YAKI, whose product may act downstream of the cAMP-dependent protein kinase. Genes Dev *3*, 1336-1348.
34. Toda, T., Cameron, S., Sass, P., Zoller, M., and Wigler, M. (1987). Three different genes in S. cerevisiae encode the catalytic subunits of the cAMP-dependent protein kinase. Cell *50*, 277-287.
35. Peeters, T., Louwet, W., Gelade, R., Nauwelaers, D., Thevelein, J.M., and Versele, M. (2006). Kelch-repeat proteins interacting with the Galpha protein Gpa2 bypass adenylate cyclase for direct regulation of protein kinase A in yeast. Proc Natl Acad Sci U S A *103*, 13034-13039.
36. Wilson, R.B., and Tatchell, K. (1988). SRA5 encodes the low-Km cyclic AMP phosphodiesterase of Saccharomyces cerevisiae. Mol Cell Biol *8*, 505-510.
37. Smith, A., Ward, M.P., and Garrett, S. (1998). Yeast PKA represses Msn2p/Msn4p-dependent gene expression to regulate growth, stress response and glycogen accumulation. Embo J *17*, 3556-3564.
38. de Pina, M.Z., Vazquez-Meza, H., Pardo, J.P., Rendon, J.L., Villalobos-Molina, R., Riveros-Rosas, H., and Pina, E. (2008). Signaling the signal, cyclic AMP-dependent protein kinase

bioRxiv preprint doi: https://doi.org/10.1101/676270; this version posted June 30, 2019. The copyright holder for this preprint (which was not certified by peer review) is the author/funder, who has granted bioRxiv a license to display the preprint in perpetuity. It is made available under aCC-BY-NC 4.0 International license.

inhibition by insulin-formed H2O2 and reactivation by thioredoxin. J Biol Chem *283*, 12373-12386.

39. Burgoyne, J.R., Rudyk, O., Cho, H.J., Prysyazhna, O., Hathaway, N., Weeks, A., Evans, R., Ng, T., Schroder, K., Brandes, R.P., et al. (2015). Deficient angiogenesis in redox-dead Cys17Ser PKARIalpha knock-in mice. Nature communications *6*, 7920.
40. Tagwerker, C., Flick, K., Cui, M., Guerrero, C., Dou, Y., Auer, B., Baldi, P., Huang, L., and Kaiser, P. (2006). A tandem affinity tag for two-step purification under fully denaturing conditions: application in ubiquitin profiling and protein complex identification combined with in vivocross-linking. Mol Cell Proteomics *5*, 737-748.
41. Burgoyne, J.R., Oviosu, O., and Eaton, P. (2013). The PEG-switch assay: a fast semi-quantitative method to determine protein reversible cysteine oxidation. J Pharmacol Toxicol Methods *68*, 297-301.
42. Humphries, K.M., Deal, M.S., and Taylor, S.S. (2005). Enhanced dephosphorylation of cAMP-dependent protein kinase by oxidation and thiol modification. J Biol Chem *280*, 2750-2758.
43. Huse, M., and Kuriyan, J. (2002). The conformational plasticity of protein kinases. Cell *109*, 275-282.
44. Lamming, D.W., and Anderson, R.M. (2014). Metabolic Effects of Caloric Restriction. In eLS. (John Wiley & Sons, Ltd).
45. Enns, L.C., Morton, J.F., Treuting, P.R., Emond, M.J., Wolf, N.S., Dai, D.F., McKnight, G.S., Rabinovitch, P.S., and Ladiges, W.C. (2009). Disruption of protein kinase A in mice enhances healthy aging. PLoS One *4*, e5963.
46. Jewell, J.L., Fu, V., Hong, A.W., Yu, F.X., Meng, D., Melick, C.H., Wang, H., Lam, W.M., Yuan, H.X., Taylor, S.S., et al. (2019). GPCR signaling inhibits mTORC1 via PKA phosphorylation of Raptor. eLife *8*.
47. Yao, Y., Tsuchiyama, S., Yang, C., Bulteau, A.L., He, C., Robison, B., Tsuchiya, M., Miller, D., Briones, V., Tar, K., et al. (2015). Proteasomes, Sir2, and Hxk2 form an interconnected aging network that impinges on the AMPK/Snf1-regulated transcriptional repressor Mig1. PLoS Genet *11*, e1004968.
48. Zhang, N., Quan, Z., Rash, B., and Oliver, S.G. (2013). Synergistic effects of TOR and proteasome pathways on the yeast transcriptome and cell growth. Open biology *3*, 120137.
49. Dillin, A., Gottschling, D.E., and Nystrom, T. (2014). The good and the bad of being connected: the integrons of aging. Curr Opin Cell Biol *26*, 107-112.
50. Goulev, Y., Morlot, S., Matifas, A., Huang, B., Molin, M., Toledano, M., and Charvin, G. (2017). Nonlinear feedback drives homeostatic plasticity in H2O2 stress response. eLife *6*, 23791.
51. Woo, H.A., Yim, S.H., Shin, D.H., Kang, D., Yu, D.Y., and Rhee, S.G. (2010). Inactivation of peroxiredoxin I by phosphorylation allows localized H(2)O(2) accumulation for cell signaling. Cell *140*, 517-528.
52. Wood, Z.A., Poole, L.B., and Karplus, P.A. (2003). Peroxiredoxin evolution and the regulation of hydrogen peroxide signaling. Science *300*, 650-653.
53. Delaunay, A., Pflieger, D., Barrault, M.B., Vinh, J., and Toledano, M.B. (2002). A thiol peroxidase is an H2O2 receptor and redox-transducer in gene activation. Cell *111*, 471-481.
54. Veal, E.A., Underwood, Z.E., Tomalin, L.E., Morgan, B., and Pillay, C.S. (2017). Hyperoxidation of peroxiredoxins: Gain or loss of function? Antioxid Redox Signal.
55. Humphries, K.M., Juliano, C., and Taylor, S.S. (2002). Regulation of cAMP-dependent protein kinase activity by glutathionylation. J Biol Chem *277*, 43505-43511.
56. Burgoyne, J.R., Madhani, M., Cuello, F., Charles, R.L., Brennan, J.P., Schroder, E., Browning, D.D., and Eaton, P. (2007). Cysteine redox sensor in PKGIa enables oxidant-induced activation. Science *317*, 1393-1397.
57. Klaus, A., Zorman, S., Berthier, A., Polge, C., Ramirez, S., Michelland, S., Seve, M., Vertommen, D., Rider, M., Lentze, N., et al. (2013). Glutathione S-transferases interact with AMP-activated protein kinase: evidence for S-glutathionylation and activation in vitro. PLoS One *8*, e62497.

bioRxiv preprint doi: https://doi.org/10.1101/676270; this version posted June 30, 2019. The copyright holder for this preprint (which was not certified by peer review) is the author/funder, who has granted bioRxiv a license to display the preprint in perpetuity. It is made available under aCC-BY-NC 4.0 International license.

58. Zhang, P., Smith-Nguyen, E.V., Keshwani, M.M., Deal, M.S., Kornev, A.P., and Taylor, S.S. (2012). Structure and allostery of the PKA RIIbeta tetrameric holoenzyme. Science *335*, 712-716.
59. Peeters, K., Van Leemputte, F., Fischer, B., Bonini, B.M., Quezada, H., Tsytlonok, M., Haesen, D., Vanthienen, W., Bernardes, N., Gonzalez-Blas, C.B., et al. (2017). Fructose-1,6-bisphosphate couples glycolytic flux to activation of Ras. Nature communications *8*, 922.
60. Brachmann, C.B., Davies, A., Cost, G.J., Caputo, E., Li, J., Hieter, P., and Boeke, J.D. (1998). Designer deletion strains derived from *Saccharomyces cerevisiae* S288C: a useful set of strains and plasmids for PCR-mediated gene disruption and other applications. Yeast *14*, 115-132.
61. Giaever, G., Chu, A.M., Ni, L., Connelly, C., Riles, L., Veronneau, S., Dow, S., Lucau-Danila, A., Anderson, K., Andre, B., et al. (2002). Functional profiling of the *Saccharomyces cerevisiae* genome. Nature *418*, 387-391.
62. Li, Z., Vizeacoumar, F.J., Bahr, S., Li, J., Warringer, J., Vizeacoumar, F.S., Min, R., Vandersluis, B., Bellay, J., Devit, M., et al. (2011). Systematic exploration of essential yeast gene function with temperature-sensitive mutants. Nature biotechnology *29*, 361-367.
63. Caballero, A., Ugidos, A., Liu, B., Oling, D., Kvint, K., Hao, X., Mignat, C., Nachin, L., Molin, M., and Nystrom, T. (2011). Absence of mitochondrial translation control proteins extends life span by activating sirtuin-dependent silencing. Molecular cell *42*, 390-400.
64. Botstein, D., Falco, S.C., Stewart, S.E., Brennan, M., Scherer, S., Stinchcomb, D.T., Struhl, K., and Davis, R.W. (1979). Sterile host yeasts (SHY): a eukaryotic system of biological containment for recombinant DNA experiments. Gene *8*, 17-24.
65. Tanaka, K., Nakafuku, M., Tamanoi, F., Kaziro, Y., Matsumoto, K., and Toh-e, A. (1990). IRA2, a second gene of Saccharomyces cerevisiae that encodes a protein with a domain homologous to mammalian ras GTPase-activating protein. Mol Cell Biol *10*, 4303-4313.
66. Christianson, T.W., Sikorski, R.S., Dante, M., Shero, J.H., and Hieter, P. (1992). Multifunctional yeast high-copy-number shuttle vectors. Gene *110*, 119-122.
67. Hlavata, L., Aguilaniu, H., Pichova, A., and Nystrom, T. (2003). The oncogenic RAS2(val19) mutation locks respiration, independently of PKA, in a mode prone to generate ROS. EMBO J *22*, 3337-3345.
68. Sikorski, R.S., and Hieter, P. (1989). A system of shuttle vectors and yeast host strains designed for efficient manipulation of DNA in *Saccharomyces cerevisiae*. Genetics *122*, 19-27.
69. Voordeckers, K., Kimpe, M., Haesendonckx, S., Louwet, W., Versele, M., and Thevelein, J.M. (2011). Yeast 3-phosphoinositide-dependent protein kinase-1 (PDK1) orthologs Pkh1-3 differentially regulate phosphorylation of protein kinase A (PKA) and the protein kinase B (PKB)/S6K ortholog Sch9. J Biol Chem *286*, 22017-22027.
70. Biteau, B., Labarre, J., and Toledano, M.B. (2003). ATP-dependent reduction of cysteine-sulphinic acid by *S. cerevisiae* sulphiredoxin. Nature *425*, 980-984.
71. Bartels, D.J., Mitchell, D.A., Dong, X., and Deschenes, R.J. (1999). Erf2, a novel gene product that affects the localization and palmitoylation of Ras2 in Saccharomyces cerevisiae. Mol Cell Biol *19*, 6775-6787.
72. Gietz, R.D., and Sugino, A. (1988). New yeast-*Escherichia coli* shuttle vectors constructed with in vitro mutagenized yeast genes lacking six-base pair restriction sites. Gene *74*, 527-534.
73. Pan, X., and Heitman, J. (1999). Cyclic AMP-dependent protein kinase regulates pseudohyphal differentiation in Saccharomyces cerevisiae. Mol Cell Biol *19*, 4874-4887.
74. Mayer, C., Dimopoulos, S., Rudolf, F., and Stelling, J. (2013). Using CellX to Quantify Intracellular Events. *101*, 14.22.11-14.22.20.
75. Abraham, M.J., Murtola, T., Schultz, R., Pall, S., Smith, J.C., Hess, B., and Lindahl, E. (2015). GROMACS: High performance molecular simulations through multi-level parallelism from laptops to supercomputers. SoftwareX *54*, 1932-1940.
76. Salomon-Ferrer, R., Case, D.A., and Walker, R.C. (2013). An overview of the Amber biomolecular simulation package. Wires Comput Mol Sci *3*, 198-210.

bioRxiv preprint doi: https://doi.org/10.1101/676270; this version posted June 30, 2019. The copyright holder for this preprint (which was not certified by peer review) is the author/funder, who has granted bioRxiv a license to display the preprint in perpetuity. It is made available under aCC-BY-NC 4.0 International license.

77. Goldstein, A.L., and McCusker, J.H. (1999). Three new dominant drug resistance cassettes for gene disruption in *Saccharomyces cerevisiae*. Yeast *15*, 1541-1553.
78. Costanzo, M., Baryshnikova, A., Bellay, J., Kim, Y., Spear, E.D., Sevier, C.S., Ding, H., Koh, J.L., Toufighi, K., Mostafavi, S., et al. (2010). The genetic landscape of a cell. Science *327*, 425-431.
79. Gueldener, U., Heinisch, J., Koehler, G.J., Voss, D., and Hegemann, J.H. (2002). A second set of loxP marker cassettes for Cre-mediated multiple gene knockouts in budding yeast. Nucleic Acids Res *30*, e23.
80. Longtine, M.S., McKenzie, A., 3rd, Demarini, D.J., Shah, N.G., Wach, A., Brachat, A., Philippsen, P., and Pringle, J.R. (1998). Additional modules for versatile and economical PCR-based gene deletion and modification in Saccharomyces cerevisiae. Yeast *14*, 953-961.
81. Colombo, S., and Martegani, E. (2014). Methods to study the Ras2 protein activation state and the subcellular localization of Ras-GTP in Saccharomyces cerevisiae. Methods Mol Biol *1120*, 391-405.
82. Reiter, W., Anrather, D., Dohnal, I., Pichler, P., Veis, J., Grotli, M., Posas, F., and Ammerer, G. (2012). Validation of regulated protein phosphorylation events in yeast by quantitative mass spectrometry analysis of purified proteins. Proteomics *12*, 3030-3043.
83. Rappsilber, J., Mann, M., and Ishihama, Y. (2007). Protocol for micro-purification, enrichment, pre-fractionation and storage of peptides for proteomics using StageTips. Nat Protoc *2*, 1896-1906.
84. Vizcaino, J.A., Csordas, A., del-Toro, N., Dianes, J.A., Griss, J., Lavidas, I., Mayer, G., Perez-Riverol, Y., Reisinger, F., Ternent, T., et al. (2016). 2016 update of the PRIDE database and its related tools. Nucleic Acids Res *44*, D447-456.
85. Kong, A.T., Leprevost, F.V., Avtonomov, D.M., Mellacheruvu, D., and Nesvizhskii, A.I. (2017). MSFragger: ultrafast and comprehensive peptide identification in mass spectrometry-based proteomics. Nat Methods *14*, 513-520.
86. Jacobson, M.P., Friesner, R.A., Xiang, Z., and Honig, B. (2002). On the role of the crystal environment in determining protein side-chain conformations. J Mol Biol *320*, 597-608.
87. Mashhoon, N., Carmel, G., Pflugrath, J.W., and Kuret, J. (2001). Structure of the unliganded cAMP-dependent protein kinase catalytic subunit from Saccharomyces cerevisiae. Arch Biochem Biophys *387*, 11-19.
88. Zhu, K., Borrelli, K.W., Greenwood, J.R., Day, T., Abel, R., Farid, R.S., and Harder, E. (2014). Docking covalent inhibitors: a parameter free approach to pose prediction and scoring. J Chem Inf Model *54*, 1932-1940.
89. Ponder, J.W., and Case, D.A. (2003). Force fields for protein simulations. Adv Protein Chem *66*, 27-85.
90. Darden, T., York, D., and Pedersen, L. (1993). Particle Mesh Ewald - an N.Log(N) Method for Ewald Sums in Large Systems. J Chem Phys *98*, 10089-10092.
91. Essmann, U., Perera, L., Berkowitz, M.L., Darden, T., Lee, H., and Pedersen, L.G. (1995). A Smooth Particle Mesh Ewald Method. J Chem Phys *103*, 8577-8593.
92. Berendsen, H.J.C., Postma, J.P.M., Vangunsteren, W.F., Dinola, A., and Haak, J.R. (1984). Molecular-Dynamics with Coupling to an External Bath. J Chem Phys *81*, 3684-3690.
93. Hess, B., Bekker, H., Berendsen, H.J.C., and Fraaije, J.G.E.M. (1997). LINCS: A linear constraint solver for molecular simulations. J Comput Chem *18*, 1463-1472.
94. Hoover, W.G. (1985). Canonical Dynamics - Equilibrium Phase-Space Distributions. Phys Rev A *31*, 1695-1697.
95. Parrinello, M., and Rahman, A. (1981). Polymorphic Transitions in Single-Crystals - a New Molecular-Dynamics Method. J Appl Phys *52*, 7182-7190.

bioRxiv preprint doi: https://doi.org/10.1101/676270; this version posted June 30, 2019. The copyright holder for this preprint (which was not certified by peer review) is the author/funder, who has granted bioRxiv a license to display the preprint in perpetuity. It is made available under aCC-BY-NC 4.0 International license.

Figure legends

Figure 1. The peroxiredoxin Tsa1 slows down aging in a manner dependent on catalytic cycling but independent on H_2O_2-scavenging. **A)** Life spans of wild-type or the indicated genomic *TSA1* mutant strains. **B)** H_2O_2 scavenging measured as the removal of medium H_2O_2. A representative curve for cultures to which 200 μM was added is shown. Inset shows average scavenging rates for cultures to which 400 μM was added (n=3). Error bars indicate SD. **C)** Average HyPer3 (red) or HyPer3 C199S (black) fluorescence ratio (500 nm/420 nm) in young or old wild-type or *tsa1Δ* cells in the absence of H_2O_2 or following the addition of 200 μM H_2O_2 for 10 min. Cells of about 10-12 generations of replicative age (old) or young control cells (young) were isolated by the biotin-streptavidin method. Error bars indicate standard error of the mean (n=170-619). **D)** Average HyPer3 (red) or HyPer3 C199S (black) fluorescence ratio (500 nm/420 nm) in young or old wild-type (YMM130) and o/e *TSA1* cells isolated as in **C)**. Error bars indicate standard error of the mean (n=381-579).

Figure 2. The accelerated aging and H_2O_2 sensitivity of cells lacking Tsa1 can be counteracted by reducing protein kinase A signaling. **A)** Overview of the Ras-cAMP-PKA glucose sensing pathway. Selected stimulatory (in green) and inhibitory (in red) components are shown. **B, D)** Lifespan of cells lacking Tsa1, Ras2, Pde2 or combinations thereof (n=120-293). **C)** H_2O_2 sensitivity of cells lacking Tsa1, Ras2 or both at the indicated culture density. **E)** Growth and H_2O_2 sensitivity of the indicated mutant cells overexpressing *IRA2* (mc-*IRA2*) or the vector control (control).

Figure 3. The slow growth of Ras-deficient cells can be restored by mutations preventing Tsa1 catalytic cycling and its inhibitory effect on PKA signaling. **A)** Growth rates of cells lacking Ras2, Tsa1 or both (n=3, error bars indicate SD). **B-C)** Growth rates of cells overexpressing *IRA2* in the indicated mutants of the Tsa1 catalytic cycle or the PKA signaling pathway on solid (**B**) or in liquid medium (**C**, n=3-7). **D)** Expression of the PKA repressed *CTT1* or *HSP12* genes in the indicated mutants in the Tsa1 catalytic cycle overexpressing *IRA2* (mc-*IRA2*) or not (instead expressing the vector, control, n=3±SD) sampled during mid-exponential growth. **E-F)** Growth of Tsa1-proficient or deficient (*tsa1Δ*) cells overexpressing *IRA2* (mc-*IRA2*) or *PDE2* (mc-*PDE2*), both or the corresponding vector control plasmids (control) on solid medium (**E**) or in liquid medium (**F**, n=3±SD).

Figure 4. An extra copy of the *TSA1* gene represses PKA signaling, increases H_2O_2 resistance and extends lifespan in a manner dependent on reduced PKA signaling. **A)** Accumulation of glycogen in vector control cells or cells expressing an extra copy of the *TSA1* gene as assayed by iodine vapor. **B)** Expression of Hsp12 in the indicated mutant strains. **C)** H_2O_2 resistance in the indicated mutant strains. **D)** Lifespans of cells expressing an extra copy of the *TSA1* gene or not (expressing the vector control) in combination with the deletion of *PDE2* to induce high PKA signaling (*pde2Δ*, n=92-439).

Figure 5. Tsa1 inhibits PKA activity through the glutathionylation of a conserved cysteine in a PKA catalytic subunit Tpk1. **A-B)** Ras-GTP (**A**) or cAMP (**B**) levels in the wild-type or the indicated mutant strains overexpressing *IRA2* (mc-*IRA2*) or not (expressing the vector control, control). **C)**

bioRxiv preprint doi: https://doi.org/10.1101/676270; this version posted June 30, 2019. The copyright holder for this preprint (which was not certified by peer review) is the author/funder, who has granted bioRxiv a license to display the preprint in perpetuity. It is made available under aCC-BY-NC 4.0 International license.

Spore viability of cells deficient in Ras1, Ras2, Tsa1 or combinations thereof. Viability was estimated in 32 tetrads where genotypes could be assigned to all spores (128 in total, 8-23 spores per genotype). **D)** Total time of nuclear Msn2 localization in the indicated mutant strains for 60 min following the addition of 0.3 mM H_2O_2. **E**) MS-MS spectrum showing the matching b-ion (blue) and y-ion (red) series following fragmentation of the Thr241 phosphorylated and C243 glutathionylated peptide encompassing amino acid residues Y239-K261 in Tpk1. T* = phospho-threonine, C-SSG = glutathionylated cysteine. **F)** PRM-based quantification of the indicated Thr241 and Cys243 containing Y239-K261 peptides in Tpk1, in the absence or presence of the indicated amount of H_2O_2, respectively (n=3). Error bars indicate SD. **G)** mPEG assay of the oxidation of Tpk1 following the addition of the indicated amount of H_2O_2 for 10 min. Cells were treated with H_2O_2, lysed by TCA and reduced cysteines alkylated by NEM. Following reduction by DTT, oxidized cysteines were alkylated by mPEG in half of the extract (mPEG) and to the other half NEM was added as a control (NEM).

Figure 6. Tpk1 Cys243 redox-modification and Tsa1 inhibits PKA activity by dephosphorylating and destabilizing the activation loop. **A)** Homology model of the yeast holo-PKA enzyme consisting of two Tpk1 catalytic subunits (C) and two Bcy1 regulatory subunits (R). **B)** Structure of mouse type II PKA holoenzyme used to build the yeast structural homology model [PDB ID 3TNP, [58]]. **C-F)** Amino acids in the activation loop (in red) of Tpk1 in the Thr241 phosphorylated Cys243 non-modified (**C**), Thr241 non-phosphorylated Cys243 non-modified (**D**), Thr241 non-modified Cys243 glutathionylated (**E**) and Thr241 phosphorylated Cys243 glutathionylated (**F**) states in the Tpk1 structural homology model. The backbones are colored in light blue, carbon atoms in yellow, nitrogen atoms in blue, oxygen atoms in red and phosphor atoms in scarlet. The distance between Lys233 and phosphorylated Thr241 is 9.55 Å (**c**) whereas Lys233 and non-phosphorylated Thr241 reside 10.88 Å apart (**D**). **G, I)** H_2O_2 resistance of the wild-type vector control (**G**, pRS313 or **I**, pRS403) or the indicated *TSA1*- or *tpk*-mutant strains. Strains in **I)** carry pRS316-*TPK1* or pRS316-*tpk1C243A* as the only PKA catalytic subunit (genomic *tpk1Δtpk2Δtpk3Δ* deletions). **H**) Glutathionylation of Tpk1-HB in *tpk2Δtpk3Δ (TSA1)* and *tpk2Δtpk3Δ tsa1Δ (tsa1Δ)* as assayed by anti-glutathione immunoblot of immunoprecipitated Tpk1-HB in the absence of or 10 min following the addition of 0.4 mM H_2O_2. Extracts were separated under non-reducing (NR) or reducing (R) conditions. **J)** H_2O_2 resistance of *tpk1Δtpk2Δtpk3Δ* and *tpk1Δtpk2Δtpk3Δtsa1Δ* cells transformed with pRS313-*TPK1* or pRS313-*tpk1T241A* as indicated.

Figure 7. Model of the mechanisms by which altered peroxiredoxin levels impacts on aging. In the first mechanism peroxiredoxin-dependent redox-signaling impacts in an unconventional manner on the PKA nutrient signaling kinase (this study) and in the other on proteostasis [18]. **A)** In wild-type cells Tsa1 catalytic cycling maintains longevity by decreasing PKA-dependent nutrient signaling leading to the stimulation of maintenance but at the expense of growth. **B)** In contrast, in cells lacking Tsa1 nutrient signaling is aberrantly increased leading to reduced maintenance and increased growth. **C)** Enforced expression of the peroxiredoxin Tsa1 slows down aging both by repressing nutrient signaling (this study) and by stimulating protein quality control mechanisms to reduce the levels of damaged and aggregated protein [18].

bioRxiv preprint doi: https://doi.org/10.1101/676270; this version posted June 30, 2019. The copyright holder for this preprint (which was not certified by peer review) is the author/funder, who has granted bioRxiv a license to display the preprint in perpetuity. It is made available under aCC-BY-NC 4.0 International license.

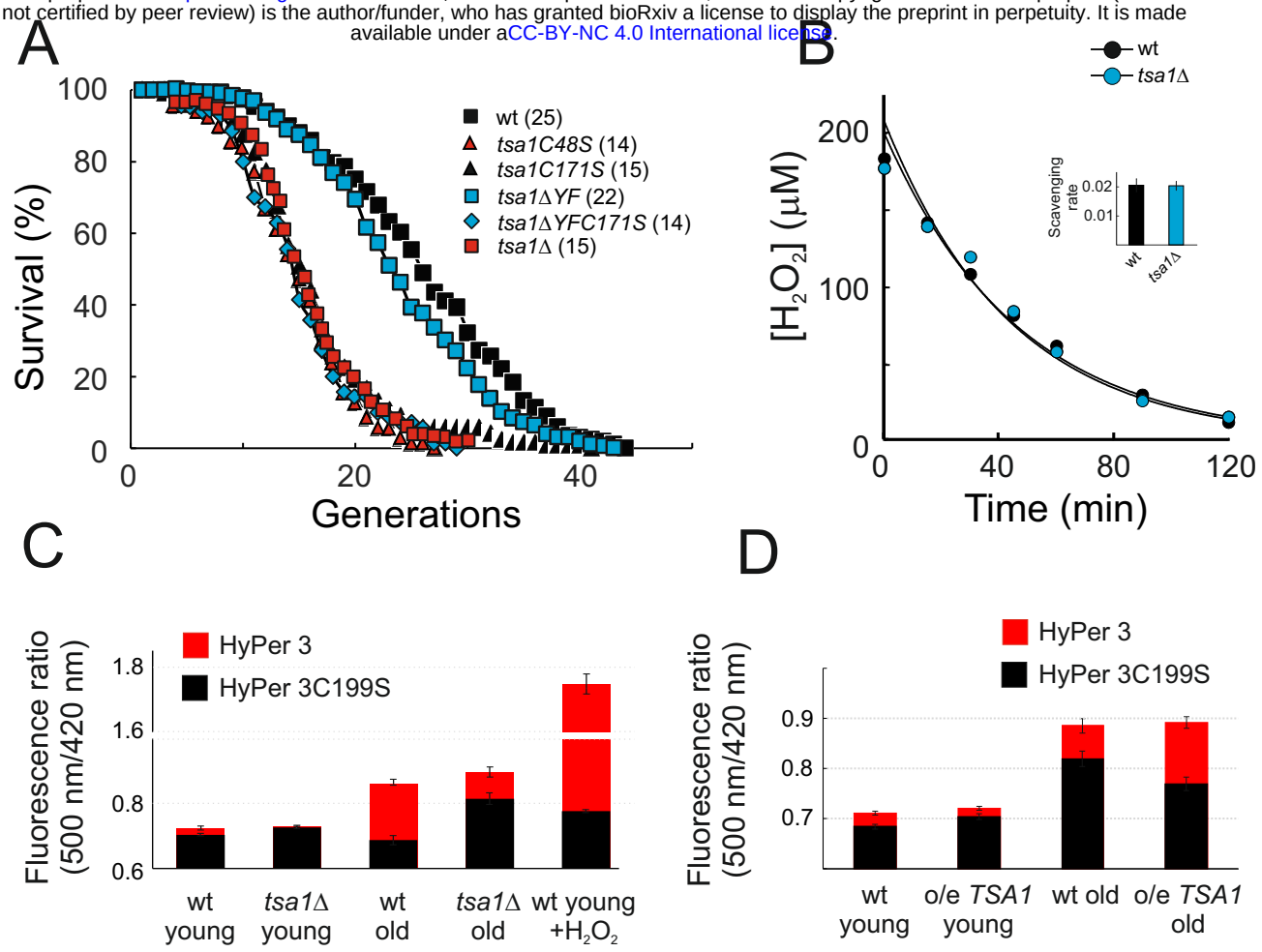

Figure 1, Roger et al

bioRxiv preprint doi: https://doi.org/10.1101/676270; this version posted June 30, 2019. The copyright holder for this preprint (which was not certified by peer review) is the author/funder, who has granted bioRxiv a license to display the preprint in perpetuity. It is made available under aCC-BY-NC 4.0 International license.

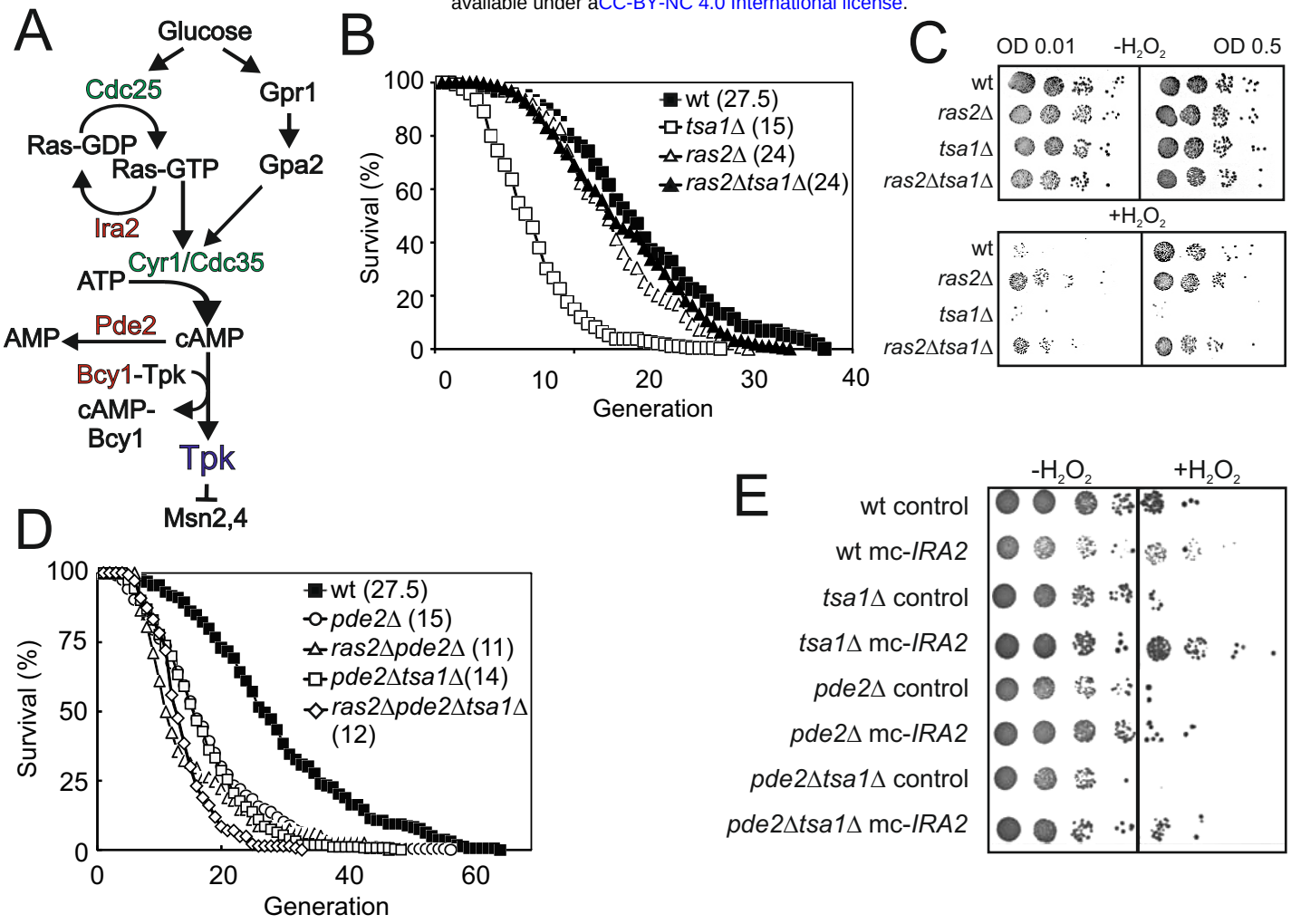

Figure 2, Roger et al

bioRxiv preprint doi: https://doi.org/10.1101/676270; this version posted June 30, 2019. The copyright holder for this preprint (which was not certified by peer review) is the author/funder, who has granted bioRxiv a license to display the preprint in perpetuity. It is made available under aCC-BY-NC 4.0 International license.

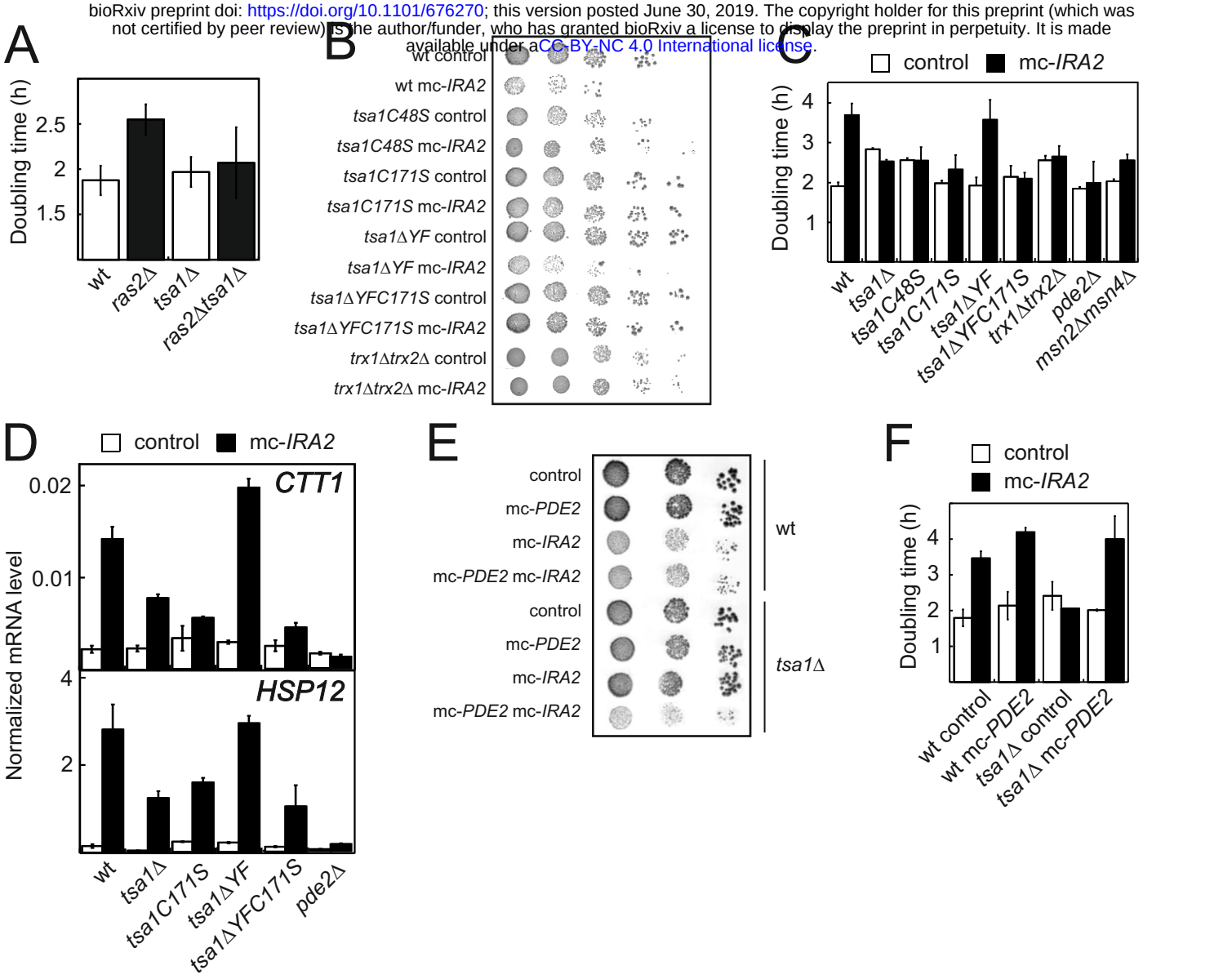

Figure 3, Roger et al

bioRxiv preprint doi: https://doi.org/10.1101/676270; this version posted June 30, 2019. The copyright holder for this preprint (which was not certified by peer review) is the author/funder, who has granted bioRxiv a license to display the preprint in perpetuity. It is made available under aCC-BY-NC 4.0 International license.

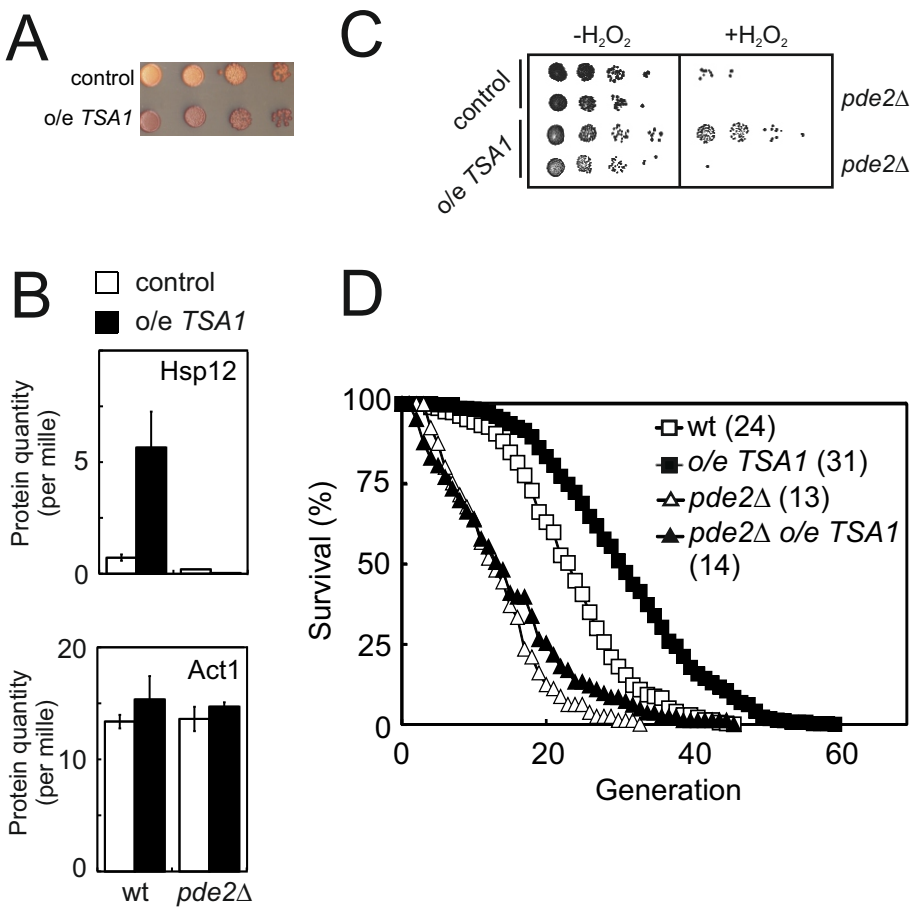

Figure 4, Roger et al

bioRxiv preprint doi: https://doi.org/10.1101/676270; this version posted June 30, 2019. The copyright holder for this preprint (which was not certified by peer review) is the author/funder, who has granted bioRxiv a license to display the preprint in perpetuity. It is made available under aCC-BY-NC 4.0 International license.

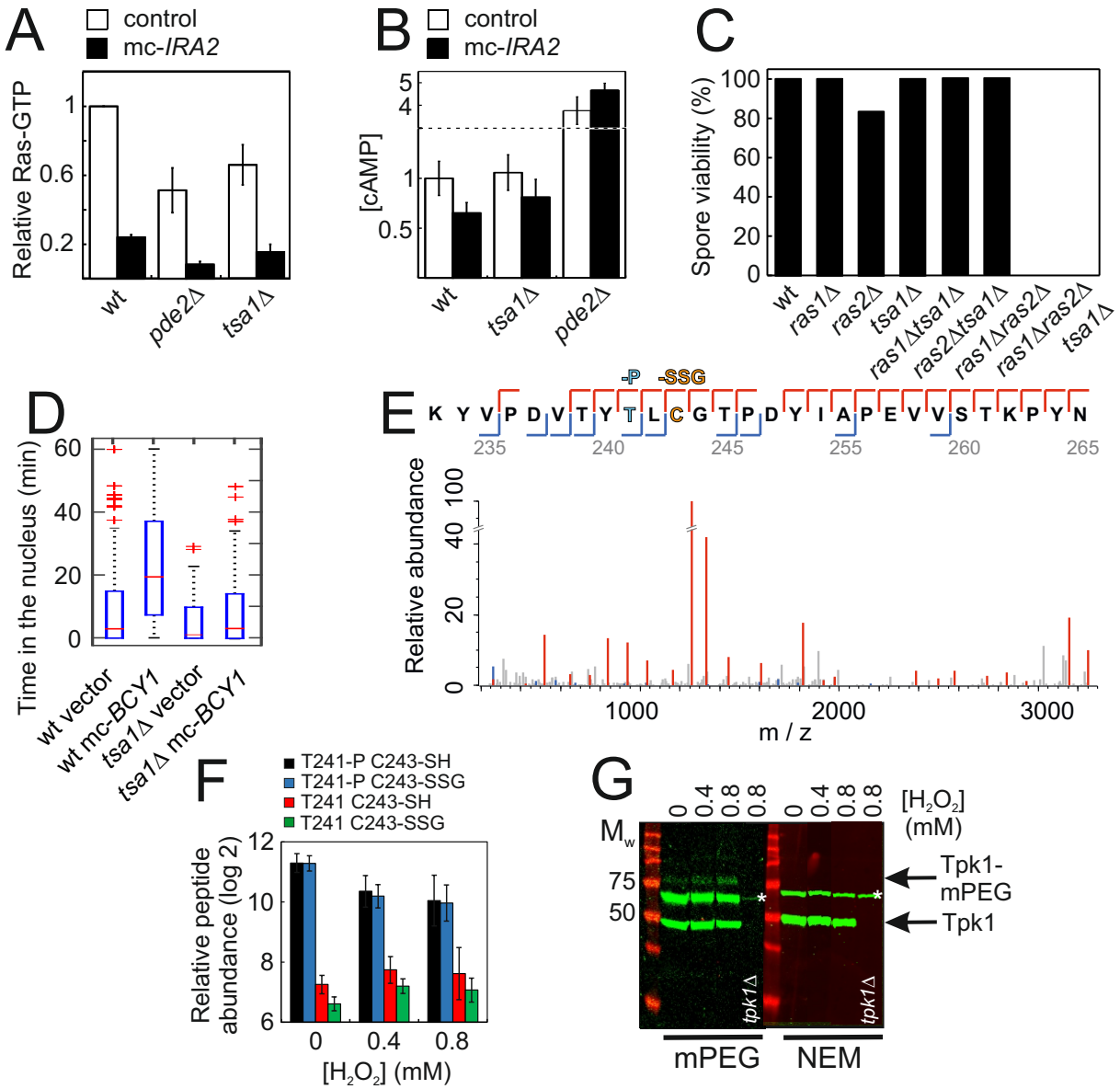

Figure 5, Roger et al

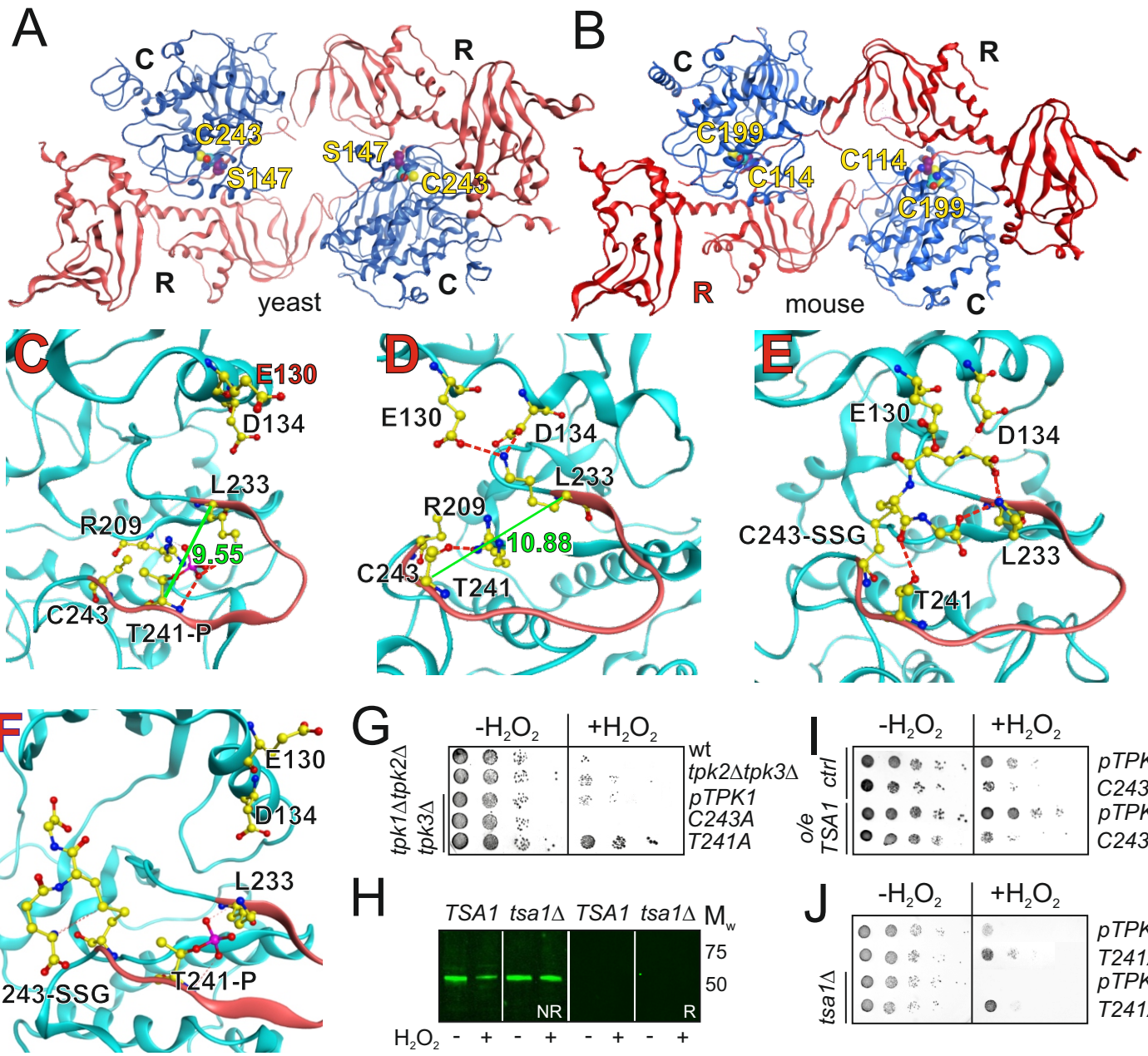

Figure 6, Roger et al

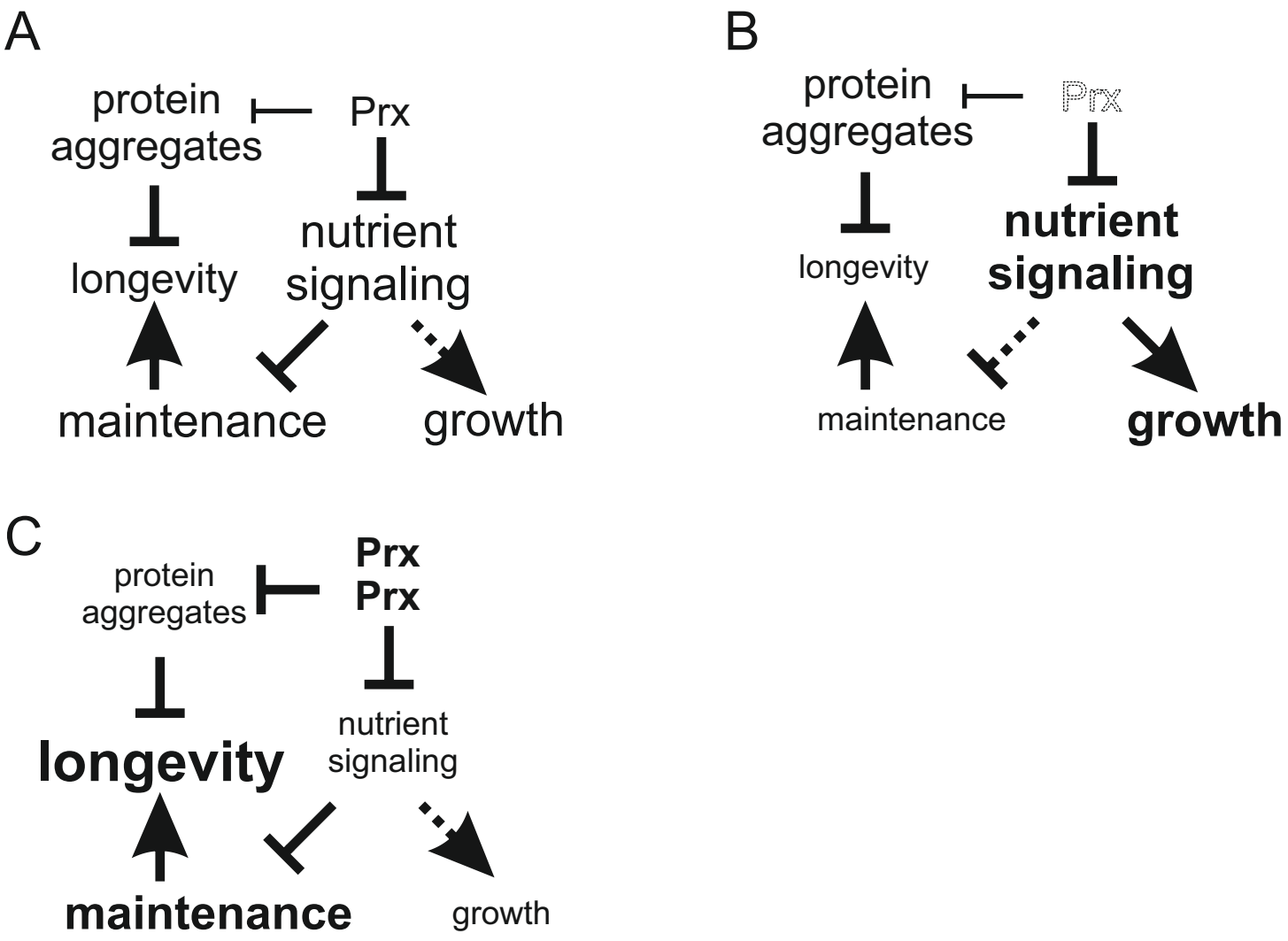

Figure 7, Roger et al

bioRxiv preprint doi: https://doi.org/10.1101/676270; this version posted June 30, 2019. The copyright holder for this preprint (which was not certified by peer review) is the author/funder, who has granted bioRxiv a license to display the preprint in perpetuity. It is made available under aCC-BY-NC 4.0 International license.

STAR✲METHODS

KEY RESOURCES TABLE

REAGENT or RESOURCE	SOURCE	IDENTIFIER
Antibodies		
Mouse monoclonal anti-Tpk1	Santa Cruz Biotechnology	Sc-374592, RRID: AB_10990730
Goat polyclonal anti-Bcy1	Santa Cruz Biotechnology	Sc-6734, RRID: AB_671758
Rabbit IgG (anti-ProtA)	Sigma Aldrich	I5006, RRID: AB_1163659
Goat polyclonal anti-Ras2	Santa Cruz Biotechnology	Sc-6759, RRID: AB_672465
Mouse monoclonal anti-Glutathione [D8]	Abcam	ab19534, RRID: AB_880243
Bacterial and Virus Strains		
E. coli BL21 strain expressing pGEX2T-1-GST-RBD	This study, [59]	
Chemicals, Peptides, and Recombinant Proteins		
G418	Acros Organics	Cat #: 329400050
ClonNAT	Werner Bioagents	Cat #: 5.005.000
Hygromycin B	Formedium	Cat #: HYG5000
Phleomycin	Sigma Aldrich	P9564
5-fluoroorotic acid	Sigma Aldrich	F5013
EZ-Link Sulfo-NHS-LC Biotin	Thermo Fisher	Cat #: 21335
Trichloroacetic acid	Sigma Aldrich	Cat #: T6399
KSCN	Sigma Aldrich	Cat #: P2713
$(NH_4)_2Fe(SO_4)_2$ • 6 H2O	Sigma Aldrich	Cat #: 215406
TRIzol Reagent	Thermo Fisher	Cat #: 15596026
DNase		
cOmplete Mini EDTA-free protease inhibitor	Roche Applied Science	Cat #: 11873580001
Glutathione-S-Transferase-Raf1-Binding-Domain (GST-RBD)	This study, [59]	
Glutathione Sepharose beads		
12% Bis-Tris NUPAGE gels	Thermo Fisher	Cat #: NP0349BOX
MOPS running buffer	Thermo Fisher	Cat #: NP0001
Immobilon-FL PVDF membrane	Millipore	Cat #: IPFL00010
Ni^{2+}-Sepharose beads	GE Healthcare	Cat #: 17-5318-06
Trypsin Gold, mass spectrometry grade	Promega	Cat #: V5280
N-ethylmaleimide	Sigma-Aldrich	Cat #: E3876
Methoxypolyethylene glycol maleimide (mPEG)	Sigma Aldrich	Cat #: 63187
10% Criterion TGX Precast Midi Protein Gel	Bio-Rad	Cat #: 5671034
Peptide Retention Time Calibration Mixture	Pierce, Thermo Fisher	Cat #: 88320
Critical Commercial Assays		
PureLink RNA Mini kit	Thermo-Fisher	Cat #: 12183025
QuantiTect Reverse Transcription Kit	Qiagen	Cat #: 205313
iQ SYBR Green Supermix	BioRad	Cat #: 170-8882
LANCE cAMP 384 kit	Perkin Elmer	Cat #: AD0262
Deposited Data		
Tpk1 MS-data	PRIDE	PXD012617
Experimental Models: Organisms/Strains		

bioRxiv preprint doi: https://doi.org/10.1101/676270; this version posted June 30, 2019. The copyright holder for this preprint (which was not certified by peer review) is the author/funder, who has granted bioRxiv a license to display the preprint in perpetuity. It is made available under aCC-BY-NC 4.0 International license.

BY4742, wt	[60]	MAT **alpha** *his3Δ1 leu2Δ0 lys2Δ0 ura3Δ0*
YMM145, *tsa1C48S*	[24]	BY4742 *tsa1C48S*
YMM146, *tsa1C171S*	[24]	BY4742 *tsa1C171S*
YMM147, *tsa1ΔYF*	[24]	BY4742 *tsa1(1-184)*
YMM148, *tsa1C171SΔYF*	[24]	BY4742 *tsa1(1-184)C171S*
YMM114, *tsa1Δ*	[11]	BY4742 *tsa1Δ::natMX4*
YMM113, *ras2Δ*	[11]	BY4742 *ras2Δ::kanMX4*
YMM170, *ras2Δtsa1Δ*	This study	BY4742 *ras2Δ::kanMX4 tsa1Δ::natMX4*
BY4742, *pde2Δ*	Research Genetics, [61]	BY4742 *pde2Δ::kanMX4*
YMM171, *ras2Δpde2Δ*	This study	BY4742 *ras2Δ::kanMX4 pde2Δ::hphMX4*
YMM172, *pde2Δtsa1Δ*	This study	BY4742 *pde2Δ::kanMX4 tsa1Δ::natMX4*
YMM173, *ras2Δpde2Δtsa1Δ*	This study	BY4742 *ras2Δ::kanMX4 pde2Δ::hphMX4 tsa1Δ::natMX4*
YMM174, *msn2Δmsn4Δ*	This study	BY4742 *msn2Δ::hphMX4 msn4Δ::natMX4*
YMM143, *trx1Δtrx2Δ*	[24]	BY4742 *trx1Δ::hphMX4 trx2Δ::natMX4*
YMM130, wt control	[18]	MAT **alpha** *his3Δ1::pRS403, leu2Δ0 lys2Δ0 ura3Δ0*
o/e *TSA1*	[18]	MAT **alpha** *his3Δ1::pRS403-Myc-TSA1, leu2Δ0 lys2Δ0 ura3Δ0*
YMM175, *pde2Δ control*	This study	MAT **alpha** *his3Δ1::pRS403, leu2Δ0 lys2Δ0 ura3Δ0 pde2Δ::kanMX4*
YMM176, *pde2Δ* o/e *TSA1*	This study	MAT **alpha** *his3Δ1::pRS403-Myc-TSA1, leu2Δ0 lys2Δ0 ura3Δ0 pde2Δ::kanMX4*

bioRxiv preprint doi: https://doi.org/10.1101/676270; this version posted June 30, 2019. The copyright holder for this preprint (which was not certified by peer review) is the author/funder, who has granted bioRxiv a license to display the preprint in perpetuity. It is made available under aCC-BY-NC 4.0 International license.

YMM177	This study	**MAT a**, *his3Δ1 leu2Δ0 lys2Δ0 ura3Δ0 ras1Δ::hphMX4*
YMM178	This study	BY-2n *met15Δ0/MET15 lys2Δ0/LYS2 tpk1Δ::kanMX4/TPK1 tpk2Δ::natMX4/TPK2 tpk3Δ::hphMX4/TPK3*
YMM179, *tpk2Δtpk3Δ*	This study	BY4742 *tpk2Δ::natMX4 tpk3Δ::hphMX4*
YMM180, *tpk1Δtpk2Δtpk3Δ pTPK1-URA*	This study	BY4742 *tpk1Δ::kanMX4 tpk2Δ::natMX4 tpk3Δ::hphMX4 pRS316-TPK1*
YMM181, *tpk1Δtpk2Δtpk3Δ pTPK1-URA vector control*	This study	BY4742 *tpk1Δ::kanMX4 tpk2Δ::natMX4 tpk3Δ::hphMX4 pRS313 pTPK1-URA3*
YMM182, *tpk1Δtpk2Δtpk3Δ pTPK1-URA pTPK1*	This study	BY4742 *tpk1Δ::kanMX4 tpk2Δ::natMX4 tpk3Δ::hphMX4 pRS313-TPK1 pTPK1-URA3*
YMM183, *tpk1Δtpk2Δtpk3Δ pTPK1-URA3 ptpk1C243A*	This study	BY4742 *tpk1Δ::kanMX4 tpk2Δ::natMX4 tpk3Δ::hphMX4 pRS313-tpk1C243A pTPK1-URA3*
YMM184, *tpk1Δtpk2Δtpk3Δ pTPK1-URA3 ptpk1C243D*	This study	BY4742 *tpk1Δ::kanMX4 tpk2Δ::natMX4 tpk3Δ::hphMX4 pRS313-tpk1C243D pTPK1-URA3*
YMM185, *tpk1Δtpk2Δtpk3Δ pTPK1-URA3 ptpk1T241A*	This study	BY4742 *tpk1Δ::kanMX4 tpk2Δ::natMX4 tpk3Δ::hphMX4 pRS313-tpk1T241A pTPK1-URA3*
YMM186, *tpk1Δtpk2Δtpk3Δ pTPK1*	This study	BY4742 *tpk1Δ::kanMX4 tpk2Δ::natMX4 tpk3Δ::hphMX4 pRS313-TPK1*

bioRxiv preprint doi: https://doi.org/10.1101/676270; this version posted June 30, 2019. The copyright holder for this preprint (which was not certified by peer review) is the author/funder, who has granted bioRxiv a license to display the preprint in perpetuity. It is made available under aCC-BY-NC 4.0 International license.

YMM187, *tpk1Δtpk2Δtpk3Δ ptpk1C243A*	This study	BY4742 *tpk1Δ::kanMX4 tpk2Δ::natMX4 tpk3Δ::hphMX4 pRS313-tpk1C243A*
YMM188, *tpk1Δtpk2Δtpk3Δ ptpk1C243D*	This study	BY4742 *tpk1Δ::kanMX4 tpk2Δ::natMX4 tpk3Δ::hphMX4 pRS313-tpk1C243D*
YMM189, *tpk1Δtpk2Δtpk3Δ ptpk1T241A*	This study	BY4742 *tpk1Δ::kanMX4 tpk2Δ::natMX4 tpk3Δ::hphMX4 pRS313-tpk1T241A*
YMM190, *ras2Δtrx1Δtrx2Δ*	This study	BY4742 *ras2Δ::kanMX4 trx1Δ::hphMX4 trx2Δ::natMX4*
YMM191	This study	BY4741 *tsa1Δ::bleMX4*
YMM192, *tpk2Δtpk3Δtsa1Δ*	This study	BY4741 *tpk2Δ::natMX4 tpk3Δ::hphMX4 tsa1Δ::bleMX4*
BY4741, wt	[60]	MAT a *his3Δ1 leu2Δ0 met15Δ0 ura3Δ0*
cdc25-1	Charlie Boone, [62]	BY4741, *cdc25-1-3'UTR(CDC25)-::kanMX4-3'UTR(SYS1)*
WR1832, *TPK1-HBH tpk2Δtpk3Δ*	This study	BY4742 *TPK1-HBH::TRP1 tpk2Δ::natMX4 tpk3Δ::hphMX4 trp1Δ::kanMX4*
yCP101, *tpk1Δtpk2Δtpk3Δ pTPK1-URA vector control*	This study	MAT **a** *his3Δ1::pRS403, leu2Δ0 lys2Δ0 ura3Δ0 tpk1Δ::kanMX4 tpk2Δ::natMX4 tpk3Δ::hphMX4 pRS316-TPK1*
yCP102, *tpk1Δtpk2Δtpk3Δ ptpk1C243A-URA vector control*	This study	MAT **alpha** *his3Δ1::pRS403, leu2Δ0 lys2Δ0 ura3Δ0 tpk1Δ::kanMX4 tpk2Δ::natMX4 tpk3Δ::hphMX4 pRS316-tpk1C243A*

bioRxiv preprint doi: https://doi.org/10.1101/676270; this version posted June 30, 2019. The copyright holder for this preprint (which was not certified by peer review) is the author/funder, who has granted bioRxiv a license to display the preprint in perpetuity. It is made available under aCC-BY-NC 4.0 International license.

yCP103, *tpk1Δtpk2Δtpk3Δ pTPK1-URA* o/e *TSA1*	This study	MAT **alpha** *his3Δ1::pRS403-myc-TSA1, leu2Δ0 lys2Δ0 ura3Δ0 tpk1Δ::kanMX4 tpk2Δ::natMX4 tpk3Δ::hphMX4 pRS316-TPK1*
yCP104, *tpk1Δtpk2Δtpk3Δ ptpk1C243A-URA* o/e *TSA1*	This study	MAT **alpha** *his3Δ1::pRS403-myc-TSA1, leu2Δ0 lys2Δ0 ura3Δ0 tpk1Δ::kanMX4 tpk2Δ::natMX4 tpk3Δ::hphMX4* pRS316-*tpk1C243A*
yCP105, *tpk1Δtpk2Δtpk3Δtsa1Δ pTPK1*	This study	BY4742 *tpk1Δ::kanMX4 tpk2Δ::natMX4 tpk3Δ::hphMX4 tsa1Δ::bleMX4 pRS313-TPK1*
yCP106, *tpk1Δtpk2Δtpk3Δtsa1Δ ptpk1T241A*	This study	BY4742 *tpk1Δ::kanMX4 tpk2Δ::natMX4 tpk3Δ::hphMX4 tsa1Δ::bleMX4 pRS313-tpk1T241A*
yCP107, *TPK1-HBH tpk2Δtpk3Δtsa1Δ*	This study	BY4742 *TPK1-HBH::TRP1 tpk2Δ::natMX4 tpk3Δ::hphMX4 trp1Δ::kanMX4 tsa1Δ::bleMX4*
Oligonucleotides		
ACT1F	[63]	For Q-PCR of *ACT1* CTGCCGGTATTG ACCAAACT
ACT1R	[63]	For Q-PCR of *ACT1* CGGTGAATTTCC TTTTGCATT
CTT1F	This study	For Q-PCR of *CTT1* GCTTCTCAATAC TCAAGACCAG
CTT1R	This study	For Q-PCR of *CTT1* GCGGCGTATGTA ATATCACTC
HSP12F	[63]	For Q-PCR of *HSP12* AGGTCGCTGGTA AGGTTC
HSP12R	[63]	For Q-PCR of *HSP12* ATCGTTCAACTT GGACTTGG
Recombinant DNA		

bioRxiv preprint doi: https://doi.org/10.1101/676270; this version posted June 30, 2019. The copyright holder for this preprint (which was not certified by peer review) is the author/funder, who has granted bioRxiv a license to display the preprint in perpetuity. It is made available under aCC-BY-NC 4.0 International license.

pHyPer3 (pRS416-*GPD-HyPer3*)	This study, [25]	HyPer3 codon-optimized for yeast, in yeast CEN/ARS, pGPD, *URA3* plasmid
pHyPer3C199S (pRS416-*GPD-HyPer3C199S*)	This study, [25]	HyPer3C199S
yEP24	[64]	yeast 2μ, *URA3* vector
pKF56	[65]	*IRA2* in yEP24
pRS425	[66]	yeast 2μ, *LEU2* vector
yEP13-*PDE2*	[67]	*PDE2* in yeast 2μ, *LEU2* plasmid
pRS313	[68]	yeast CEN/ARS, *HIS3* empty vector
pRS313-*TPK1*	[69]	*TPK1* in pRS313
pRS313-*tpk1C243A*	This study	*tpk1C243A* in pRS313
pRS313-*tpk1C243D*	This study	*tpk1C243D* in pRS313
pRS313-*tpk1T241A*	This study	*tpk1T241A* in pRS313
pRS316	[68]	yeast CEN/ARS, *URA3* empty vector
pRS316- *myc-TSA1*	[70]	Myc-*TSA1* in pRS316
pRS316- *myc-tsa1C48S*	[11]	Myc-*tsa1C48S* in pRS316
pRS316- *myc-tsa1C171S*	[11]	Myc-*tsa1C171S* in pRS316
pRS315	[68]	yeast CEN/ARS, *LEU2* empty vector
B561 (pRS315-*RAS2G19V*)	[71]	*RAS2G19V* in pRS315
pRS315-ProtA	This study	ProteinA in pRS315
pRS315-*TRX2-ProteinA*	[24]	*TRX2-ProtA* in pRS315
pRS315-*trx2C34S-ProteinA*	This study	*trx2C34S-ProtA* in pRS315
pRS315-*trx2C31SC34S-ProteinA*	This study	*trx2C31SC34S-ProtA* in pRS315
yEPlac195	[72]	yeast 2μ, *URA3* vector
pXP1	[73]	*TPK1* in yEPlac195
p*TPK1-URA3 (*pRS316-*TPK1)*	Karin Voordeckers	*TPK1* in pRS316
p*tpk1C243A-URA3*	This study	*tpk1C243A* in pRS316
Software and Algorithms		
MATLAB	Mathworks	version 2016b
CellX	[74]	
Scrödinger Suite	Schrödinger LLC	
GROMACS	[75]	
Amber tools	[76]	

CONTACT FOR REAGENT AND RESOURCES SHARING

Please contact M.M. (mikael.molin@chalmers.se) for reagents and resources generated in this study

EXPERIMENTAL MODEL AND SUBJECT DETAILS

Yeast (*Saccharomyces cerevisiae*) is the experimental model used in this study.

bioRxiv preprint doi: https://doi.org/10.1101/676270; this version posted June 30, 2019. The copyright holder for this preprint (which was not certified by peer review) is the author/funder, who has granted bioRxiv a license to display the preprint in perpetuity. It is made available under aCC-BY-NC 4.0 International license.

METHOD DETAILS

Strains and growth conditions

Strains and plasmids are listed in the Key Resources Table. The strains used in this study are derivatives of BY4741/BY4742. Strains were grown at 30°C in YPD 2% glucose (w/v) or in Yeast Nitrogen Base defined medium containing 2% glucose and complete supplement mixture (CSM) lacking the appropriate amino acids (Formedium) as described previously [11]. To check the segregation of deletion markers in tetrad dissections YPD medium supplied with the following chemicals was used to check segregation of the dominant markers: *kanMX4* (G418 200 µg/ml), *natMX4* (ClonNAT 100 µg/ml), *hphMX4* (Hygromycin B 300 µg/ml), *bleMX4* (Phleomycin 40 µg/ml). To counterselect the p*TPK1-URA3* plasmid cells were grown in defined glucose CSM –HIS, 5-FOA medium containing YNB, glucose and CSM –URA, HIS; 50 mg/l uracil and 1 g/l 5-fluoroorotic acid.

Strain and plasmid constructions

Strains YMM170 (*ras2*Δ*tsa1*Δ*)* and YMM172 (*pde2*Δ*tsa1*Δ*)* were constructed by crossing strain YMM114 to BY4741 *ras2*Δ*::kanMX4* and BY4741 *pde2*Δ*::kanMX4* [Research Genetics, [61]], respectively, and selecting for Mat alpha, methionine prototrophic, lysine auxotrophic, G418 resistant and nourseothricin resistant progeny. Strains YMM171 and YMM173 were constructed by crossing a BY4741 *pde2*Δ*::hphMX4* {*pde2*Δ*::kanMX4* from the deletion collection [Research Genetics, [61]] marker-switched [77] to *pde2*Δ*::hphMX4* to strain YMM170 (*ras2*Δ*tsa1*Δ) and selecting for Mat alpha, methionine prototrophic, lysine auxotrophic, G418 resistant, hygromycin resistant and nourseothricin sensitive (YMM171 *ras2*Δ*pde2*Δ) or nourseothricin resistant (YMM173 *ras2*Δ*pde2*Δ*tsa1*Δ) progeny. Strains YMM174 (*msn2*Δ*msn4*Δ), YMM175 (*pde2*Δ) and YMM176 (*pde2*Δ o/e *TSA1*) were constructed by crossing BY4741 *msn2*Δ*msn4*Δ [63] or BY4741 *pde2*Δ*::kanMX4* [Research Genetics, [61]] to strains YMM130 or BY4742 *his3*Δ*1::pRS403-Myc-TSA1*, respectively and selecting for Mat alpha, methionine prototrophic, lysine auxotrophic, histidine auxotrophic, hygromycin- and nourseothricin-resistant progeny (YMM174) or Mat alpha, methionine prototrophic, lysine auxotrophic, G418 resistant and histidine prototrophic progeny (YMM174 and YMM175). Strain YMM177 was constructed by marker-switching [77] a Mat a *ras1*Δ*::kanMX4* spore, obtained from crossing strain BY4741 *ras1*Δ*::kanMX4* [Research Genetics, [61]] to strain YMM114 and selecting for Mat a, methionine prototrophic, lysine auxotrophic and G418 resistant progeny, to *ras1*Δ*::hphMX4*. Strain YMM178 (*tpk1*Δ*/TPK1 tpk2*Δ*/TPK2 tpk3*Δ*/TPK3*) was constructed by crossing a BY4742 *tpk1*Δ*::kanMX4 tpk2*Δ*::natMX4* strain to a BY4741 *tpk3*Δ*::hphMX4* strain {*tpk3*Δ*::kanMX4* from the deletion collection [Research Genetics, [61]] marker-switched (Goldstein and McCusker, 1999) to *tpk3*Δ*::hphMX4* resulting in a *tpk1Δ/TPK1 tpk2Δ/TPK2 tpk3Δ/TPK3* heterozygous diploid strain. A Mat alpha, nourseothricin- and hygromycin-resistant spore constitutes strain YMM179. The BY4742 *tpk1*Δ*::kanMX4 tpk2*Δ*::natMX4* strain was constructed by introducing *tpk2*Δ*::natMX4* PCR amplified from a BY4742 *tpk2*Δ*::natMX4* strain [78] into strain BY4741 *tpk1*Δ*::kanMX4* [Research Genetics, [61]] selecting for nourseothricin- and G418-resistance and verifying the deletion by diagnostic PCR. A BY4742 *tpk1*Δ*tpk2*Δ*tpk3*Δ p*TPK1-URA3* haploid strain (YMM180) was constructed by transforming strain YMM177 with plasmid p*TPK1-URA3* and sporulating the strain selecting for a Mat alpha methionine prototrophic, lysine auxotrophic, G418-, nourseothricin-, hygromycin B-resistant and uracil auxotrophic progeny. Strains YMM181-YMM185 were constructed by transforming strain YMM179 with plasmids pRS313 (YMM181), pRS313-*TPK1* (YMM182), pRS313-*tpk1C243A* (YMM183) and pRS313-*tpk1C243D* (YMM184) and pRS313-*tpk1T241A* (YMM185). Counterselecting p*TPK1-URA3* on 5-FOA medium resulted in strains

bioRxiv preprint doi: https://doi.org/10.1101/676270; this version posted June 30, 2019. The copyright holder for this preprint (which was not certified by peer review) is the author/funder, who has granted bioRxiv a license to display the preprint in perpetuity. It is made available under aCC-BY-NC 4.0 International license.

YMM186 (BY4742 *tpk1*Δ*tpk2*Δ*tpk3*Δ pRS313-*TPK1*), YMM187 (BY4742 *tpk1*Δ*tpk2*Δ*tpk3*Δ pRS313-*tpk1C243A*), YMM188 (BY4742 *tpk1*Δ*tpk2*Δ*tpk3*Δ pRS313-*tpk1C243D*) and yMM189 (BY4742 *tpk1*Δ*tpk2*Δ*tpk3*Δ pRS313-*tpk1T241A*), respectively. Strain YMM190 (*ras2*Δ*trx1*Δ*trx2*Δ) was constructed by crossing strain YMM113 (*ras2*Δ) to strain YMM143 (*trx1*Δ*trx2*Δ) selecting for Mat alpha, methionine prototrophic, lysine auxotrophic, G418-, nourseothricin- and hygromycin B-resistant progeny. Strain YMM191 was constructed by marker-switching strain BY4741 *tsa1*Δ*::kanMX4* [Research Genetics, [61]] into BY4741 *tsa1*Δ*::bleMX4* using a bleMX4 cassette PCR amplified from plasmid pUG66 [79] using primers PR78 and PR79 [77]. Strain yMM192 was constructed by crossing strains yMM179 and yMM191 selecting for a Mat a, nourseothricin+, hygromycin+ and phleomycin+ spore. Strain WR1832 was constructed by first introducing PCR amplified *trp1Δ::kanMX4* DNA [80] into strain YMM179, verification of cassette integration by PCR and loss of the ability to grow without tryptophan supplement and next by *HBH::TRP1* C-terminal tagging of *TPK1* and PCR based verification as described [40]. Strains yCP101-yCP104 were constructed by crossing Mat a *his3Δ1::pRS403* or *his3Δ1::pRS403-myc-TSA1* spores, obtained in crosses generating strains yMM175 above, either to strain yMM182 or to strain yMM186 also carrying plasmid *pRS316-tpk1C243A*. Methionine prototrophic, lysine auxotrophic, histidine prototrophic, 5-FOA-sensitive, G418+, nourseothricin+ and hygromycin B+ progeny obtained in these crosses constitute strains yCP101-yCP104 listed in Table S1. Strains yCP105 and yCP106 were constructed by crossing strains yMM186 (p*TPK1*) or yMM189 (p*tpk1T241A*), respectively, to strain yMM192 selecting for Mat alpha, Met+, Lys-, G418+, Nat+, Hyg+, Phleomycin+, His+ progeny. Strain yCP107 was constructed by crossing strain WR1832 to yMM192 and selecting for Mat alpha, Met+, Lys-, G418+, Nat+, Hyg+, Phleomycin+, Trp+ progeny.

Plasmids pRS313-*tpk1C243A*, pRS313-*tpk1C243D*, pRS313-*tpk1T241A* and pRS316-*tpk1C243A*, were constructed by site directed mutagenesis of the pRS313-*TPK1* or pRS316-*TPK1* plasmids (Eurofins Genomics). Plasmids pRS315-*trx1C34S*-ProtA and pRS315-*trx2C31SC34S*-ProtA were constructed by site-directed mutagenesis of plasmid pRS315-*TRX2*-ProtA (GenScript). The correct sequence of all plasmids constructed was verified by sequencing.

Global H_2O_2 scavenging in the medium

Medium peroxide determinations were performed using a ferrithiocyanate spectrophotometric assay (Molin et al., 2007). After bolus addition of H_2O_2, 100 µL sample aliquots were withdrawn and cultures were arrested by the addition of 1 ml ice-cold 10% TCA. After pelleting cells 180 mM KSCN and 1.4 mM $Fe(NH_4)_2(SO_4)_2$ final concentrations were added to the supernatants. Absorbance at 480 nm was subsequently determined and compared to equally TCA-treated H_2O_2 standards diluted in medium.

Isolation of old cells

Old cells were obtained as previously described by sorting biotin-labeled mother cells using the MagnaBind streptavidin system (Sinclair and Guarente, 1997). Briefly, mid-exponential phase cells were labeled with EZ-Link Sulfo-NHS-LC Biotin and grown overnight in minimal media (CSM-His). The cells were incubated with streptavidin-conjugated magnetic beads for 2 h and then sorted magnetically with the unlabeled cells being washed away. Sorted cells were then grown overnight and the streptavidin labeling procedure was repeated before sorting one last time. After sorting the cells were incubated for 1 h in CSM-His media at 30 ◦C for recovery before microscopy.

Measurements of cytoplasmic H_2O_2 using HyPer3

bioRxiv preprint doi: https://doi.org/10.1101/676270; this version posted June 30, 2019. The copyright holder for this preprint (which was not certified by peer review) is the author/funder, who has granted bioRxiv a license to display the preprint in perpetuity. It is made available under aCC-BY-NC 4.0 International license.

Fluorescence of the ratiometric probe HyPer-3 (Bilan et al., 2013) was acquired using an Olympus IX81 motorized microscope with a PlanApoN 60x/1.42 Oil objective and a 12-bit Hamamatsu camera. Shifts in the fluorescence intensities were acquired with excitation around 500 nm (485/20 nm) and 420 nm (427/10 nm filter) and an emission filter around 520 nm (Fura 2 filter). For bolus addition of H_2O_2, cells in midexponential phase were incubated with 0.6 mM H_2O_2 for 10 min and immediately imaged.

Image Analysis

Image and signal analysis was performed using the MATLAB toolbox 2016b. Cell segmentation is performed with the CellX algorithm using the bright-field channel. The fluorescent intensity data was obtained from fluorescent images and data is presented as the median 500 nm fluorescent signal normalized to the median fluorescent 420 nm signal by dividing the latter with the former.

Lifespan Analyses

Lifespan analyses were performed as previously described by counting the number of daughters produced in a cohort of mother cells (Erjavec et al., 2007).

Spot tests

H_2O_2 resistance was tested with mid-exponential-phase (A_{600}=0.5, 5 × 10^6 cells/ml) cells that were diluted (x5, x50, x500, x5000, x50000) and spotted onto SD media containing 0 to 1 mM H_2O_2 or YPD media containing 0 to 2 mM. The plates were incubated at 30 ◦C for 3 days. For glycogen accumulation, plates incubated for 2 days at 30 ◦C were exposed to iodine-bead fumes for 2.5 min and scanned immediately.

Quantitative Real-Time PCR Analysis

Cell cultures were harvested in mid-exponential phase and resuspended in 1 ml Trizol Reagent (Invitrogen) and homogenized with silica beads by Fast prep (6.5 m/s, 30 sec, interval 2.5min, 4 ◦C). RNA was extracted using phenol chloroform extraction and precipitated with sodium acetate/ethanol. The pellet was treated with DNase for 30min followed by heat-inactivation of the enzyme. The RNA was purified with Invitrogen PureLink RNA Mini Kit columns and converted to cDNA following the QIAGEN QuantiTect Reverse Transcription Kit. Q-PCR was performed with 50ng cDNA by using BioRad iQ SYBR Green Supermix and quantified with the BioRad iCycler, iQ5. Relative levels of mRNA were calculated by using cycle times of *ACT1* as a reference gene.

2D-PAGE

Protein synthesis rates of the indicated proteins were determined in ^{35}S-Methionine labelled protein extracts separated by two-dimensional polyacrylamide gel electrophoresis as described (Maillet et al., 1996; Molin et al., 2011). Tsa1 sulfinylation was determined by comparing levels of sulfinylated Tsa1 (Tsa1-SOOH) to non-sulfinylated Tsa1 on silver-stained 2D gels as described (Molin et al., 2011).

Measurement of Ras2-GTP *in vivo*

Ras2-GTP level were measured as a ratio between Ras2-GTP and total Ras2 as described previously [59, 81]. Mid-exponential phase yeast cells were harvested and lysed with glass- beads in Fast-prep (6.0 m/s, 20sec, interval 2.5 min) in lysis buffer [50 mM Tris-HCl, 200 mM NaCl, 2.5 mM $MgCl_2$, 10% glycerol, 1% Triton X100, cOmplete Protease inhibitor EDTA-free]. The supernatant with 1.5mg

bioRxiv preprint doi: https://doi.org/10.1101/676270; this version posted June 30, 2019. The copyright holder for this preprint (which was not certified by peer review) is the author/funder, who has granted bioRxiv a license to display the preprint in perpetuity. It is made available under aCC-BY-NC 4.0 International license.

of total protein was incubated with a bed volume 50 µL of glutathione S-transferase (GST)-RBD fusion protein pre-bound to glutathione-Sepharose for 1 h at 4 ◦C and washed three times with lysis buffer by centrifugation. For elution the beads were boiled for 5 min at 98 ◦C in SDS-sample buffer (6% SDS, 62.5 mM Tris-HCl pH 8.7, 30% Glycerol, 0.75% β-mercaptoethanol). Through western blotting, Ras2-GTP and total Ras2 proteins were detected with anti-Ras2 antibodies. Determination of ratios between Ras2-GTP and total Ras2 was performed by ImageJ.

cAMP measurement

cAMP measurements were performed as previously described (Caballero et al., 2011; Parts et al., 2011). 2×10^8 cells grown to midexponential phase were pelleted, washed, and resuspended in 1 ml cold milliQ water. Metabolites were extracted by adding 1.2 ml TCA (0.5 M) and occasional vigourous vortexing while samples were kept on ice for 15 min. TCA was removed by ether extraction. cAMP levels were determined by the LANCE cAMP 384 kit in 40 µL total reactions and by comparing to the standards supplied. The values for cAMP were normalized to the wild type level.

Spore viability

The viability of spores segregating in the sporulation and dissection of a heterozygous diploid *ras1*Δ*::hphMX4/RAS1 ras2*Δ*::kanMX4/RAS2 tsa1*Δ*::natMX4/TSA1* strain obtained by crossing strain YMM176 (*ras1*Δ*::hphMX4*) to strain YMM170 (BY4742 *ras2*Δ*::kanMX4 tsa1*Δ*::natMX4*) was analyzed after 4 days of incubation at 30°C in 32 tetrads where 1) all markers analyzed (*hphMX4, kanMX4, natMX4, MET15, LYS2*) segregated 2:2, 2) the exact genotypes of all spores were possible to deduce from this information and 3) the genotypes of dead spores were assigned based on markers present in the other spores dissected from the same tetrads. Similarly, spore viability of spores segregating in a heterozygous diploid *tpk1*Δ*::kanMX4/TPK1 tpk2*Δ*::natMX4/TPK2 tpk3*Δ*::hphMX4/TPK3 tsa1*Δ*::bleMX4/TSA1*, obtained by crossing strain YMM191 (BY4741 *tsa1*Δ*::bleMX4*) to strain YMM186 (BY4742 *tpk1*Δ*::kanMX4 tpk2*Δ*::natMX4 tpk3*Δ*::hphMX4* expressing pRS313-*TPK1*), was analyzed in 43 tetrads where all chromosomal markers analyzed (*kanMX4, natMX4, hphMX4, bleMX4, MET15, LYS2*) segregated 2:2. The ability to grow in the absence of histidine supplementation (-HIS) was taken as an indication that the pRS313-*TPK1* plasmid was present.

Immunoblot analysis

Immunoblot analysis of selected proteins was performed as described previously [11, 70]. Prior to separation on 12% Bis-Tris NuPAGE gels using an XCell SureLock MiniCell (Invitrogen) in NuPAGE MOPS running buffer as recommended by the supplier protein extracts were heated in Laemlii buffer (pH 8.7) either in the presence of β-mercaptoethanol (5%, reducing) or not (non-reducing) as indicated. Transfer to Immobilon-FL PVDF membranes was done using an XCell II Blot Module kit. Membranes were analyzed by the Odyssey infrared imaging system (LI-COR biosciences) as recommended by the suppliers.

Glutathionylation of Tpk1 was assayed using anti-glutathione immunoblot on Tpk1-HB immunoprecipitated by Ni^{2+}-Sepharose beads following a simplified protocol similar to that used during MS sample preparation (see below).

Growth conditions for MS analysis

Cells were grown at 30°C in yeast extract/peptone (YP) medium, containing 2% glucose as carbon source. Three independent experimental replicates were performed for each experimental condition.

bioRxiv preprint doi: https://doi.org/10.1101/676270; this version posted June 30, 2019. The copyright holder for this preprint (which was not certified by peer review) is the author/funder, who has granted bioRxiv a license to display the preprint in perpetuity. It is made available under aCC-BY-NC 4.0 International license.

For each replicate, we inoculated 750ml YPD cultures, which were incubated (with shaking) overnight until OD600 = 1. Oxidative stress was induced by adding 0.4 mM or 0.8 mM (final concentration) H_2O_2 for 10 minutes.

Mass spectrometric sample preparation

HB (poly histidine, biotinylation signal) tandem affinity purifications were performed as described elsewhere [82]. Cells were harvested by filtration and immediately deep-frozen in liquid N_2. Cells were grinded using a SPEX Freezer Mill 6870 (SPEXSamplePrep, Metuchen, NJ, USA) with the following settings: 7 cycles: 3 min breakage (15 CPS), 3 min cooling, resuspended in buffer 1 (6 M guanidine HCl, 50 mM Tris pH8.0, 5 mM NaF, 1 mM PMSF, 0.1% Tween, cOmplete Protease inhibitor cocktail, pH 8) and cleared of debris by centrifugation 13.500 x g, 15 min, 4°C. Cleared extracts were incubated (4 hours, room temperature) with Ni^{2+}-Sepharose beads, washed with urea buffer (8M urea, 50mM sodium phosphate buffer pH8.0, 300mM NaCl, 0.1% Tween20) and urea buffer pH 6.3. Proteins were eluted in urea buffer pH 4.3 containing 10mM EDTA, incubated overnight with streptavidin-agarose beads, washed using urea wash buffer containing 1% SDS and urea wash buffer without SDS. Beads were washed five times with 50 mM ammonium bicarbonate (ABC). Cys-residues were alkylated with IAA (25% w/w of the estimated amount of protein). Excess IAA was washed out by ABC. Proteins were digested with 300 ng trypsin at 37°C overnight. Digestion was stopped with trifluoroacetic acid (0.5% final concentration) and the peptides were desalted using C18 Stagetips [83]. 50 fmol of the Peptide Retention Time Calibration Mixture was spiked in each sample for quality control.

Mass spectrometry analysis of Tpk1

Peptides were separated on an Ultimate 3000 RSLC nano-flow chromatography system (Thermo-Fisher), using a pre-column (Acclaim PepMap C_{18}, 2 cm × 0.1 mm, 5 µm, Thermo-Fisher), and a C_{18} analytical column (Acclaim PepMap C18, 50 cm × 0.75 mm, 2 µm, Thermo-Fisher). A segmented linear gradient from 2% to 35% solvent B (solvent B: 80% acetonitrile, 0.1% formic acid; solvent A: 0.1% formic acid) was applied at a flow rate of 230 nL/min over 120 min. A Proxeon nanospray flex ion source (Thermo Fisher) using coated emitter tips (New Objective) was used for ionization. The capillary temperature was set to 200°C. Peptides were analyzed on an Orbitrap Fusion Lumos Tribrid mass spectrometer (Thermo Fisher). The mass spectrometer was operated in data-dependent mode, survey scans were obtained in a mass range of 380-1500 m/z with lock mass activated, at a resolution of 120,000 at 200 m/z and an automatic gain control (AGC) target value of 4E5. The maximum cycle time was set to 2.5 s and the most abundant precursors were selected for fragmentation by high-energy collision at 30% collision energy. Fragmented precursors were excluded from further fragmentation for 30s (with +/- 5 ppm accuracy) and peptides with charge +1 or > +6 were excluded from MS/MS analysis. The most abundant Tpk1 Cys containing peptide forms have been added to an inclusion list as specified in the raw files. MS proteomics data have been deposited to the ProteomeXchange Consortium through the Proteomics Identifications database (PRIDE) partner repository [84] with the data set identifiers PXD012617.

Closed database search

Peptide identification and label free quantification (LFQ) were performed using MaxQuant (version 1.6.0.16) with default parameters. *Saccharomyces cerevisiae* reference proteome database (UniProt, version January 2017) in combination with a common laboratory contaminants database (MQ) was used for peptide spectrum matching. N-terminal acetylation, deamidation of asparagine and glutamine, oxidation of methionine, tri-oxidation and glutathionylation of cysteine and phosphorylation of serine,

bioRxiv preprint doi: https://doi.org/10.1101/676270; this version posted June 30, 2019. The copyright holder for this preprint (which was not certified by peer review) is the author/funder, who has granted bioRxiv a license to display the preprint in perpetuity. It is made available under aCC-BY-NC 4.0 International license.

threonine and tyrosine were set as variable protein modification. Carbamidomethylation of cysteine was set as fixed. A maximum of 5 variable modifications per peptide was allowed. Leucine and isoleucine were treated as indistinguishable. Enzyme specificity was set to "Trypsin/P". A maximum of 2 missed cleavages per peptide was allowed. 'Requantify' and "Match between runs" was activated. MaxLFQ (implemented in the MaxQuant package) was used for MS1-based label free quantification and normalization of protein groups.

Open search analysis of selected peptides

To screen for protein modifications in a rather unbiased manner we initially performed an open search using MSFragger in FragPipe [85]. The default open search parameters were used, with trypsin specificity, +/- 500 Da windows and oxidation of methionine and carbamidomethylation of cysteine as variable modifications. The observed mass shifts were inspected and filtered for the most abundant and relevant modifications occurring in Tpk1.

Targeted mass-spectrometry

Parallel-Reaction-Monitoring (PRM) assays were generated based on the peptide information obtained by MaxQuant. We selected Tpk1 and Tsa1 peptides for targeted relative LFQ as specified in Supplemental Table XY, datasheets 4 to 6.Peptides were separated using a 120 min gradient (HPLC setup as described above). PRM data acquisition was performed using a scheduled method with 20 min windows for each target based on the retention time determined in the shotgun-approach. Raw data were obtained on an Orbitrap Q Exactive HF-X (Thermo Fisher Scientific) mass spectrometer applying the following settings: survey scan with 60k resolution, AGC 1E6, 60 ms IT, over a range of 400 to 1400 m/z, PRM scan with 30 k resolution, AGC 1E5, 200 ms IT, isolation window of 1.0 m/z with 0.3 m/z offset, and NCE of 27%.

Wash runs were checked for potential peptide carry-over in between samples using same HPLC and MS methods. Data analysis, manual validation of all transitions (based on retention time, relative ion intensities, and mass accuracy), and relative quantification was performed in Skyline. Up to six characteristic transitions were selected for each peptide and their peak areas were summed for peptide quantification (total peak area). MS1 signals of PRTC standards were used as global standards for normalization in Skyline to account for fluctuations in instrument performance. The mean of the log2 Tpk1 non-modified peptide intensities was used to normalize Tpk1 modified peptides and Tsa1 peptides to account for differences in Tpk1 levels. Tsa1 peptide intensities (anti-log) were summed up to obtain values for relative protein abundance.

mPEG assay

To assay oxidation of the Tpk1 protein the immunoblot procedure was adapted to the mPEG-switch assay (Burgoyne et al., 2013) in the following way. Following TCA lysis, protein extraction and acetone wash dried protein was re-dissolved in buffer A (1% SDS, 10 mM EDTA, 0.1 M Tris pH 8.8), containing 50 mM NEM to alkylate reduced cysteines. Proteins were next precipitated with TCA, washed with acetone, protein pellets dried and re-dissolved in buffer A containing 5 mM DTT to reduce oxidized cysteines. Following an additional round of TCA precipitation, acetone wash and lyophilization the dry protein pellets were subsequently dissolved in buffer B (1% SDS, 10 mM EDTA, 0.1 M Tris pH 8.0) containing either 1) 2 mM methoxypolyethylene glycol maleimide (mPEG) or 2) 50 mM NEM. Extracts were next subjected to SDS-PAGE (10% Criterion TGX Gels) gel electrophoresis under reducing conditions using a Criterion cell. Proteins were blotted to membranes using a Criterion Blotter and analyzed as above.

bioRxiv preprint doi: https://doi.org/10.1101/676270; this version posted June 30, 2019. The copyright holder for this preprint (which was not certified by peer review) is the author/funder, who has granted bioRxiv a license to display the preprint in perpetuity. It is made available under aCC-BY-NC 4.0 International license.

Homology modeling

A model of the yeast PKA tetramer structure was obtained by homology modeling. The protein sequences of yeast Tpk1 (catalytic subunit of PKA) and Bcy1 (regulatory subunit of PKA) were obtained from Genbank (ID: 1023942850 and ID: 1023943330, respectively). The crystal structure of mouse PKA (PDBID: 3TNP) was used as the template for the homology calculations. The catalytic and regulatory subunits of yeast PKA and mouse PKA shares 48% and 42% sequence similarity, respectively. The homology model was built using StructurePrediction panel [86] in Schrödinger Suite (Schrödinger, LLC, New York, NY). The ClustralW method was used to align the target and template sequences in Prime, the energy-based was selected for model building method, and homo-multimer was selected for multi-template model type.

Covalent docking

Covalent docking was carried out to obtain a model for glutathionylated Tpk1. The Tpk1 crystal structure [PDB ID: 1FOT, [87]] were prepared using the Protein Preparation utility in Schrodinger to assign the correct protonation state and fix the missing side chains and loops. The glutathione was built by 3D builder and prepared by LigPre utility in Schrodinger. The Covalent-Dock panel [88] in Schrodinger was used to predict the pose of the glutathione attaching to Cys243. The reaction type was set to be disulfide formation, the docking mode was set to be thorough pose prediction, the other parameters were all set to be default. At the final step, Prime Energy was used to rank the poses of the ligand. Covalent docking was performed on dephosphorylated Tpk1 structure.

Molecular dynamics simulations

Molecular dynamics simulations were carried out to study structural changes of Tpk1 upon phosphorylation and glutathionylation. MD simulations non-modified Tpk1, Cys243 glutathionylation Tpk1, Thr241 phosphorylation Tpk1, Cys243 glutathionylation and Tpk1 phosphorylation co-existed Tpk1 were carried out. The GROMACS software [75] was used for the MD simulations and the Amber 99 [89] force field was selected to assign the parameters for different amino acid residues. The glutathionylation and phosphorylation parameters was generated from Ambertools, and incorporated into the GROMACS software.

The systems were solvated with a buffer distance of 10.0 Å TIP3P water in periodic boxes, and then 0.1 mol/L of Na+ and Cl− ions were added to adjust the systems to electroneutrality condition. Then 200 steps of the steepest descent energy minimization was carried out to remove close contacts in the obtained systems. A 2ns position-restrained simulation with a constant pressure ensemble (NPT) was performed to make sure the water molecules would reach more favorable positions. The parameters for position-restrained simulation are set to be: a time step = 1 fs, temperature = 298 K, and coupling pressure = 1 bar, Coulomb cutoff = 10 Å, Lennard-Jones cutoff = 10 Å, particle-mesh Ewald summation [90, 91] was used for longrange electrostics. The temperature and pressure was controlled by Berendsen coupling algorithm [92], with the time constants of 0.1 ps for temperature and 1.0 ps for pressure coupling. All bond lengths was contrained by the LINCS algorithm [93]. Following the position-restrained simulation, 100 ns production simulations with NPT ensemble were performed on each system for further study the protein conformational changes. In this step, the Nose−́ Hoover thermostat [94], with a time constant 0.1 ps, was used to control the temperature and the Parrinello−Rahman barostat [95], with a time constant 1.0 ps, was used to control the pressure. The other parameters were the same as those in the position-restrained simulations.

QUANTIFICATION AND STATISTICAL ANALYSIS

bioRxiv preprint doi: https://doi.org/10.1101/676270; this version posted June 30, 2019. The copyright holder for this preprint (which was not certified by peer review) is the author/funder, who has granted bioRxiv a license to display the preprint in perpetuity. It is made available under aCC-BY-NC 4.0 International license.

All experiments were repeated at least three times (biological replicates) to ensure reproducibility. Details on the number of replicates and statistical analyses performed are available below.

Figure 1. a) Lifespans were tested for statistical significance by the Mann-Whitney U test (www.socscistatistics.com/tests/mannwhitney/Default2.aspx). Lifespans of the wt (n=168) vs the *tsa1Δ* mutant (n=293), wt vs *tsa1C48S* (n=70), wt vs *tsa1C171S* (n=120), *tsa1ΔYF* (n=255) vs *tsa1ΔYFC171S* (n=70) are all different at p<0.00001. The lifespan of the *tsa1ΔYF* mutant is different from the wt at p<0.00854 whereas no significant difference was seen between the *tsa1Δ* vs *tsa1C48S* (p=0.1074), *tsa1C48S* vs *tsa1C171S* (p=0.3125), *tsa1ΔYFC171S* vs *tsa1C171S* (p=0.23014). **b)** The scavenging rates of the wt and the *tsa1Δ* mutant following the addition of 0.4 mM are not significant in a two-tailed t-test assuming equal variance (p=0.684). **c)** Fluorescence ratios 500/420 nm of the HyPer3 expressing strains are significantly different between the wt young (n=231) vs old (n=319) ($p=2.42 \times 10^{-13}$) and wt young vs wt young $+H_2O_2$ (n=202) ($p=5.27 \times 10^{-76}$) but not when comparing wt old vs *tsa1Δ* old (n=236)(p=0.101). **d)** Fluorescence ratios 500/420 nm of the HyPer3 expressing strains are neither significantly different between the wt young (n=404) vs the o/e *TSA1* young (n=579, p=0.069) nor the wt old (n=190) vs o/e *TSA1* old (n=204, p=0.755).

Figure 2. A) Lifespans of the wt (n=157) vs the *tsa1Δ* (n=293) and the *tsa1Δ* vs *ras2Δtsa1Δ* (n=283) are significantly different at p<0.00001. The lifespan of the *ras2Δ* (n=138) is not significantly different from the *ras2Δtsa1Δ* (p=0.276). **d)** Lifespans of the wt (n=157) vs the *pde2Δ* (n=120), the *ras2Δtsa1Δ* vs *ras2Δpde2Δtsa1Δ* (n=164) and the *tsa1Δ* (n=293) vs *pde2Δtsa1Δ* (n=242) are significantly different at p<0.00001. Lifespans of the *ras2Δpde2Δ* (n=124) vs *pde2Δ* are significantly different (p=0.00068) whereas the lifespans of *pde2Δ* vs *pde2Δtsa1Δ* are not significantly different (p=0.757).

Figure 3. A) Doubling times of wt and *ras2Δ* strains are significantly different at p=0.047 whereas the difference between the *tsa1Δ* and the *ras2Δtsa1Δ* is not statistically significant using a two-sided t-test assuming equal variance (p=0.77). **c)** Doubling times of control and mc-*IRA2* strains are significantly different for the wt (n=7 each, $p=7.4 \times 10^{-6}$), the *tsa1ΔYF* (n=3 and 4, respectively, p=0.0032) and *msn2Δmsn4Δ* (n=3 each, p=0.026). In none of the other strains are control and mc-*IRA2* different (*tsa1Δ* n=3 each, p=0.87; *tsa1C48S*, n=3 each, p=0.71; *tsa1C171S*, n=4 each, p=0.11; *tsa1ΔYFC171S*, n=4 each, p=0.77; *pde2Δ*, n=3 each, p=0.66; *trx1Δtrx2Δ*, n=4 each, p=0.90. d) Relative *HSP12* levels were significantly different between wt control and mc-*IRA2* strains (n=15 and 9, respectively, $p=1.0 \times 10^{-14}$), between wt mc-*IRA2* and *tsa1Δ* mc-*IRA2* strains (n=9 and 8, respectively, $p=1.9 \times 10^{-6}$), between wt mc-*IRA2* and *tsa1C171S* mc-*IRA2* strains (n=9 and 4, respectively, p=0.026), between wt mc-*IRA2* and *tsa1ΔYFC171S* mc-*IRA2* strains (n=9 and 6, respectively, p=0.00083) and between wt mc-*IRA2* and *pde2Δ* mc-*IRA2* strains (n=9 and 6, respectively, $p=4.8 \times 10^{-8}$). No significant difference was seen between wt mc-*IRA2* and *tsa1ΔYF* mc-*IRA2* strains (n=9 and 3, respectively, p=0.53). Relative *CTT1* levels were significantly different between wt control and mc-*IRA2* strains (n=24 and 21, respectively, $p=3.4 \times 10^{-13}$), between wt mc-*IRA2* and *tsa1Δ* mc-*IRA2* strains (n=21 and 6, respectively, p=0.0073), between wt mc-*IRA2* and *tsa1C171S* mc-*IRA2* strains (n=9 and 4, respectively, p=0.026), between wt mc-*IRA2* and *tsa1ΔYF* mc-*IRA2* strains (n=21 and 3, respectively, p=0.027), between wt mc-*IRA2* and *tsa1ΔYFC171S* mc-*IRA2* strains (n=21 and 6, respectively, p= $p=4.9 \times 10^{-5}$) and between wt mc-*IRA2* and *pde2Δ* mc-*IRA2* strains (n=21 and 6, respectively, $p=3.5 \times 10^{-7}$). **F)** Doubling times of control and mc-*IRA2* strains are significantly different for the wt control (n=3 each, p=0.00042), the wt o/e *PDE2* (n=3 each, p=0.00091) and for the *tsa1Δ* mc-*PDE2* strain (n=3, p=0.0058) but not for the *tsa1Δ* control strain (n=3 each, p=0.20).

bioRxiv preprint doi: https://doi.org/10.1101/676270; this version posted June 30, 2019. The copyright holder for this preprint (which was not certified by peer review) is the author/funder, who has granted bioRxiv a license to display the preprint in perpetuity. It is made available under aCC-BY-NC 4.0 International license.

Figure 4. B) Hsp12 levels are significantly different between control and o/e *TSA1* strains (n=3, p=0.033) whereas Act1 levels are not (n=3, p=0.69). **D)** Lifespans of wt control and o/e *TSA1* strains [18] are significantly different using the Mann Whitney U test (n=377 and 439 cells, p= 1.0×10^{-25}. Lifespans of *pde2Δ* control and *pde2Δ* o/e TSA1 strains are not significantly different (n=81 and 84, respectively, p=0.58).

Figure 5. A). Relative Ras2-GTP/total Ras values in the control and mc-*IRA2* are significantly different in a two tailed t-test with unequal variance for the wt (n=3, p=0.0041). Values for the *pde2Δ* control vs mc-*IRA2* (n=3, p=0.015) and the *tsa1Δ* control vs mc-*IRA2* (n=3, p=0.030) are significantly different in a two-tailed t-test with equal variance. **B)** cAMP levels are significantly different only between wt and *pde2Δ* strains (n=4 each, wt yEP24 vs pde2 yEP24, p=0.0050 and wt pKF56 vs pde2 pKF56, p=1.4 x 10^{-5}). No significant differences were seen between wt and *tsa1Δ* strains (n=4 each, wt yEP24 vs *tsa1Δ* yEP24, p=0.86 and wt pKF56 vs *tsa1Δ* pKF56 p=0.47) or between the wt yEP24 and wt pKF56 (p=0.13). E) The abundances of all the three T241-phosphorylated peptides decreased significantly upon adding either 0.4 mM or 0.8 mM H2O2 (for the C243-SH peptide p=0.05 and 0.037 respectively, for the C243-SSG peptide p=0.015 and 0.025 respectively whereas for the C243-SO_3H peptide p=0.011 and 0.0049, respectively. The quantity of the C243-SH T241 non-modified peptide did not change significantly upon the addition of 0.4 and 0.8 mM H_2O_2 (p=0.20 and 0.54, respectively) whereas the C243-SSG T241 non-modified peptide increased significantly following 0.4 mM (p=0.038) but not at 0.8 mM (p=0.17). F) The amount of Tsa1 co-purified with Tpk1 decreased significantly both following the addition of 0.4 mM vs untreated (p=0.00012) and 0.8 mM vs untreated (p=0.00016).

DATA AND SOFTWARE AVAILABILITY

All data is available from MM upon request. The Tpk1 MS data has been reposited in PRIDE with the identifier PXD012617.

bioRxiv preprint doi: https://doi.org/10.1101/676270; this version posted June 30, 2019. The copyright holder for this preprint (which was not certified by peer review) is the author/funder, who has granted bioRxiv a license to display the preprint in perpetuity. It is made available under aCC-BY-NC 4.0 International license.

Supplemental information

Peroxiredoxin promotes longevity and H_2O_2-resistance in yeast by inhibiting protein kinase A-dependent nutrient signaling

Friederike Roger, Cecilia Picazo, Chikako Asami, Wolfgang Reiter, Sarah Hanzén, Chunxia Gao, Gilles Lagniel, Niek Welkenhuysen, Jean Labarre, Thomas Nyström, Morten Grøtli, Markus Hartl and Mikael Molin

bioRxiv preprint doi: https://doi.org/10.1101/676270; this version posted June 30, 2019. The copyright holder for this preprint (which was not certified by peer review) is the author/funder, who has granted bioRxiv a license to display the preprint in perpetuity. It is made available under aCC-BY-NC 4.0 International license.

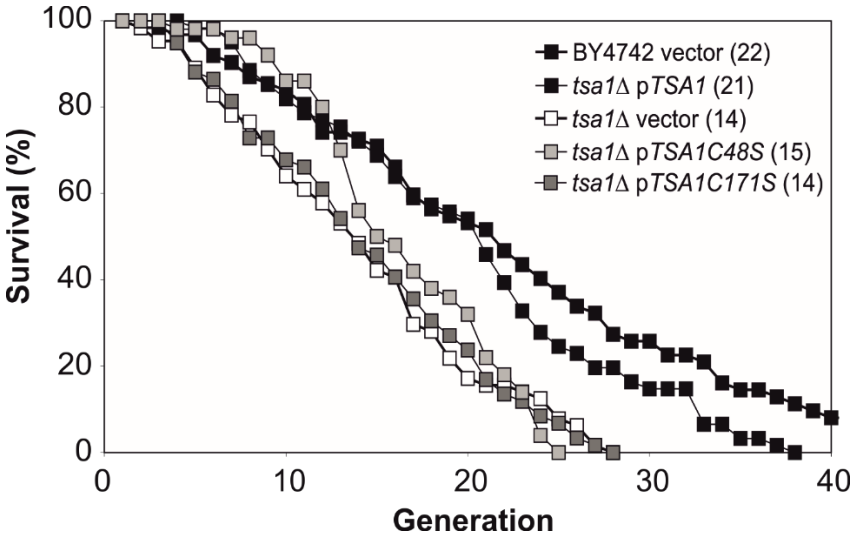

Figure S1. Related to Figure 1. Life-spans of wild-type or Tsa1-deficient cells transformed with the indicated *TSA1* mutant alleles or the vector control (pRS316, n=58-64).

bioRxiv preprint doi: https://doi.org/10.1101/676270; this version posted June 30, 2019. The copyright holder for this preprint (which was not certified by peer review) is the author/funder, who has granted bioRxiv a license to display the preprint in perpetuity. It is made available under aCC-BY-NC 4.0 International license.

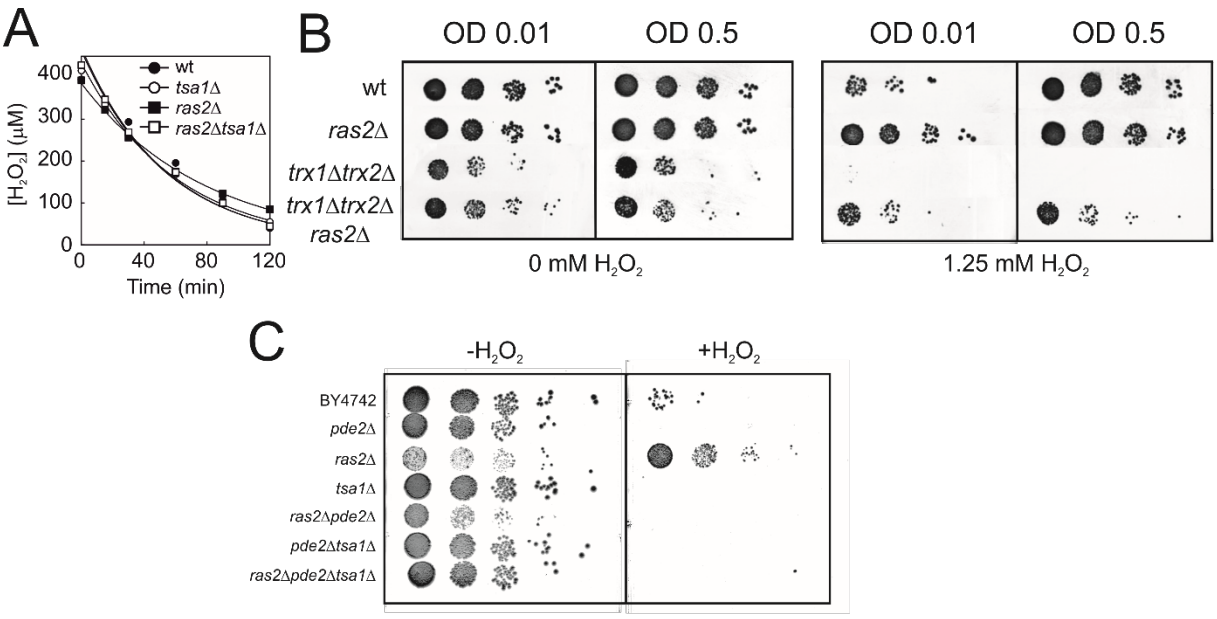

Figure S2. Related to Figure 2. Ras-deficiency counteracts the H_2O_2 sensitivity of cells lacking Tsa1 or the cytosolic thioredoxins Trx1 and Trx2 in a manner independent on increased H_2O_2 scavenging. **A)** H_2O_2 scavenging measured as the removal of medium H_2O_2. A representative curve for cultures of the indicated mutant strains to which 400 μM was added is shown. **B-C)** H_2O_2 resistance in the indicated mutant strains strains grown to early (OD0.01) and mid exponential phase (OD0.5, **B**) or OD 0.3 (**C**) and spotted onto plates with or without the indicated amounts of H_2O_2.

bioRxiv preprint doi: https://doi.org/10.1101/676270; this version posted June 30, 2019. The copyright holder for this preprint (which was not certified by peer review) is the author/funder, who has granted bioRxiv a license to display the preprint in perpetuity. It is made available under aCC-BY-NC 4.0 International license.

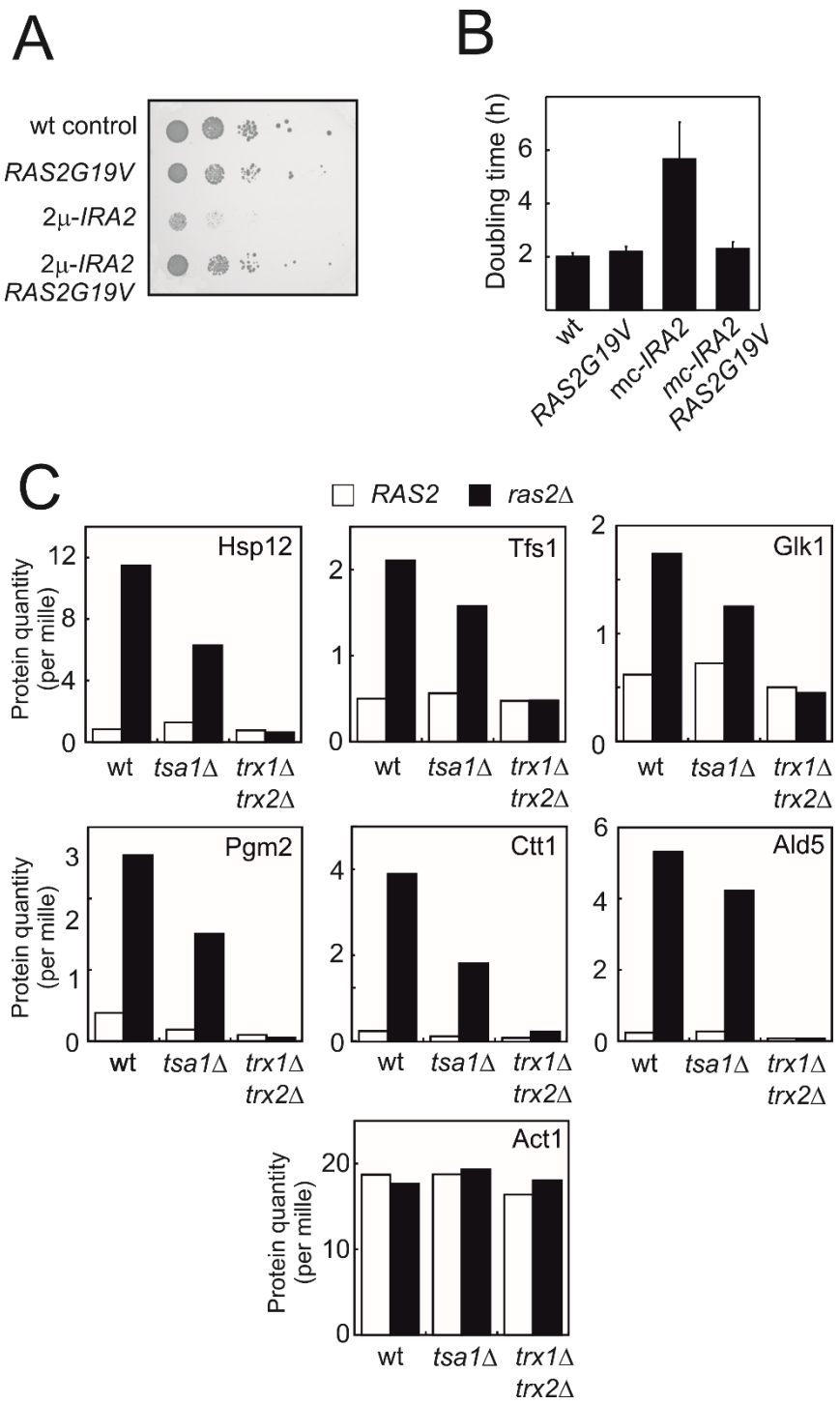

Figure S3. Related to Figure 3. Substantially reduced Ras activity slows down growth and activates Msn2 in a manner dependent on Tsa1 and the cytosolic thioredoxins. **A-B)** Growth of cells expressing the oncogenic *RAS2G19V* allele, overexpressing *IRA2* (mc-*IRA2*) or both. **C)** Expression of PKA repressed Msn2/4 targets (Hasan et al., 2002; Molin et al., 2011) in wild-type, *tsa1Δ* or *trx1Δtrx2Δ* cells deficient in *RAS2* (*ras2Δ*) or not (*RAS2*).

bioRxiv preprint doi: https://doi.org/10.1101/676270; this version posted June 30, 2019. The copyright holder for this preprint (which was not certified by peer review) is the author/funder, who has granted bioRxiv a license to display the preprint in perpetuity. It is made available under aCC-BY-NC 4.0 International license.

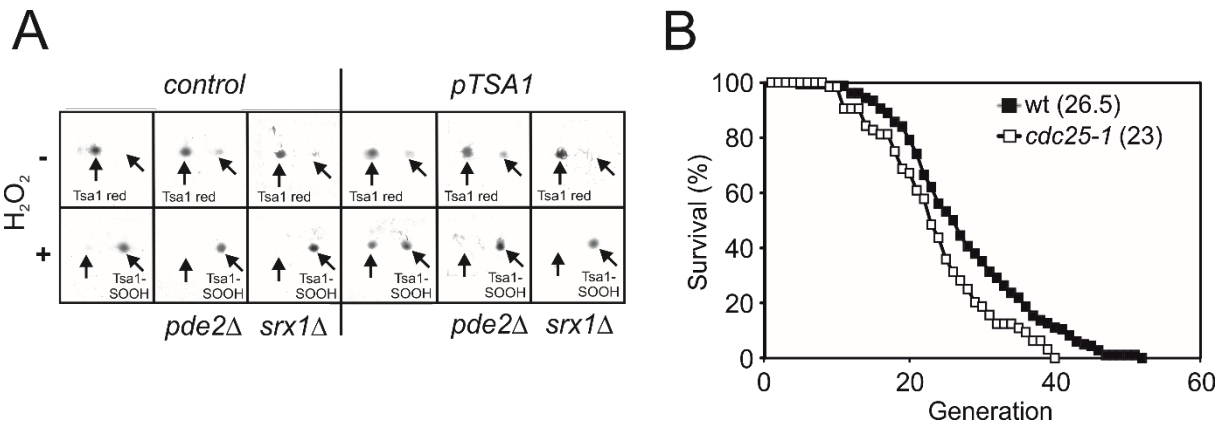

Figure S4. Related to Figure 4. Long-lived cells mildly overexpressing the *TSA1* gene moderately diminish PKA activitywhereas substantially reduced PKA signaling accelerates aging. **A)** The levels of sulfinylated Tsa1 following H_2O_2 stress is decreased in cells expressing a single extra copy of the *TSA1* gene in a manner dependent on reduced PKA signaling and Srx1. **B)** Life-spans of wild-type or *cdc25-1* mutant cells.

bioRxiv preprint doi: https://doi.org/10.1101/676270; this version posted June 30, 2019. The copyright holder for this preprint (which was not certified by peer review) is the author/funder, who has granted bioRxiv a license to display the preprint in perpetuity. It is made available under aCC-BY-NC 4.0 International license.

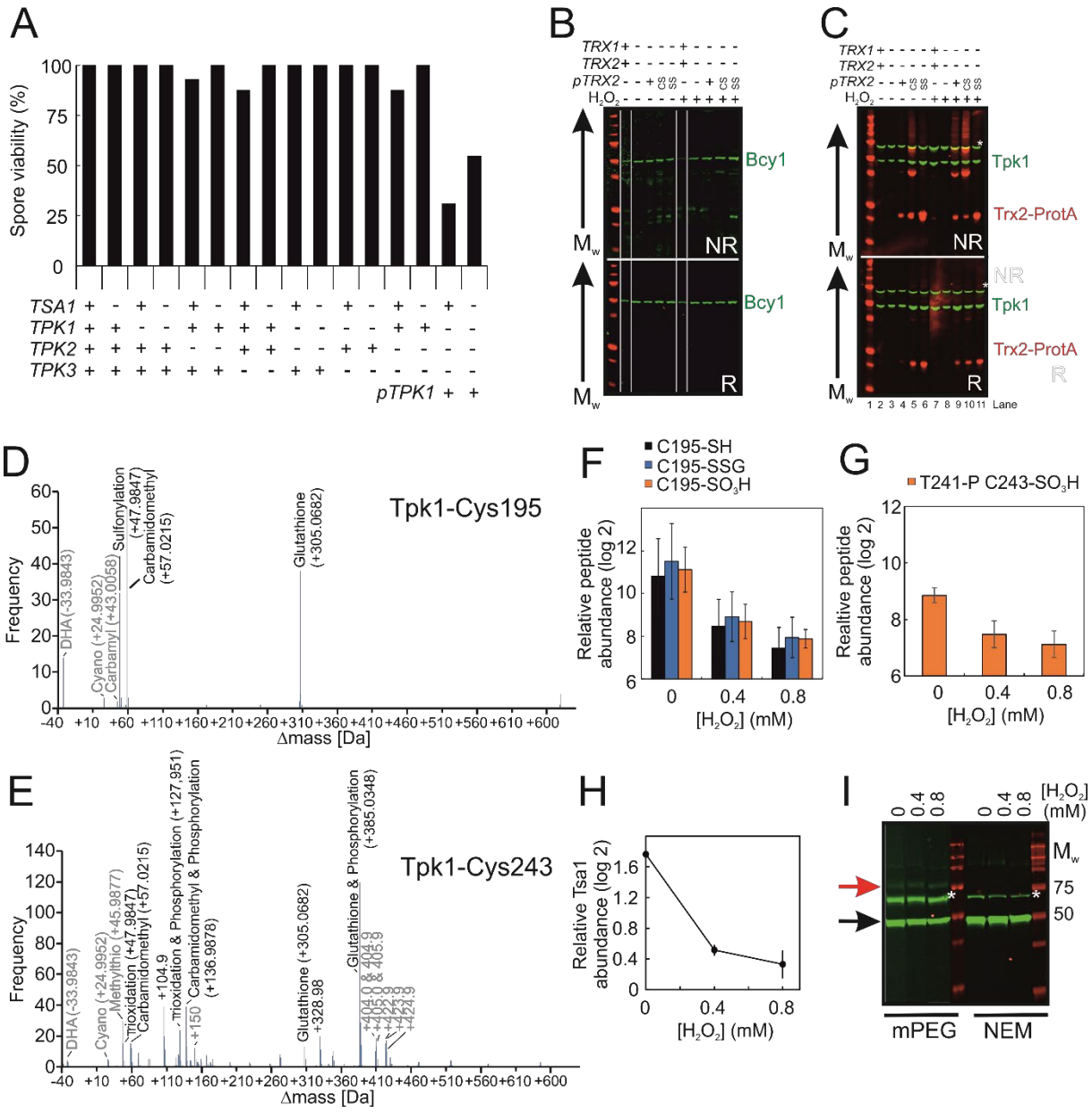

Figure S5. Related to Figure 5. Tsa1 affects PKA signaling at the level of the PKA catalytic subunits and in a manner independent on the Bcy1 regulatory subunit. **A)** Spore viability in mutants segregating in a *tsa1Δ* x *tpk1Δtpk2Δtpk3Δ* mutant cross. The *tpk1Δtpk2Δtpk3Δ* mutant was kept alive by a Tpk1-expressing plasmid (pRS313-*TPK1*). Spore viability was estimated in 43 tetrads where genotypes could be assigned to all spores (172 spores in total and in 8-15 spores per genotype). **B-C)** Bcy1 (**B**) or Tpk1 (**C**) redox immunoblots of protein extracts isolated from the indicated thioredoxin mutant strains in the absence of stress (H_2O_2 -) or following the addition of 0.4 mM H_2O_2 for 20 min (H_2O_2 +). NR = non-reducing R = reducing CS = *trx2C34S* SS = *trx2C31SC34S*. **D-E)** Mass-shifts in peptides covering the indicated Tpk1 cysteines detected using unbiased open search approaches. Tpk1-Cys195 indicates the F189-K204 peptide whereas Tpk1-Cys243 the Y239-K261 peptide. **F)** PRM-based quantification of the indicated C195 containing Tpk1 peptides (n=3). Error bars indicate SD. **G)** PRM-based quantification of the Thr241 phosphorylated and Cys243 sulfinic acid containing Y239-K261 peptide in Tpk1 (n=3). Error bars indicate SD. **H)** Relative abundance of Tsa1 co-purified with Tpk1-HB in the presence and absence of H_2O_2 as determined by the average PRM quantity of 15 different

bioRxiv preprint doi: https://doi.org/10.1101/676270; this version posted June 30, 2019. The copyright holder for this preprint (which was not certified by peer review) is the author/funder, who has granted bioRxiv a license to display the preprint in perpetuity. It is made available under aCC-BY-NC 4.0 International license.

Tsa1 peptides detected (Supplementary data Table S1). Error bars indicate SD (n=3). **I)** mPEG assay of the oxidation of Tpk1 following the addition of the indicated amount of H_2O_2 for 10 min in a *tpk1Δtpk2Δtpk3Δ* p*tpk1C243A* mutant strain. Cells were treated with H_2O_2, lysed by TCA and reduced cysteines alkylated by NEM. Following reduction by DTT, oxidized cysteines were alkylated by mPEG in half of the extract (mPEG) and to the other half NEM was added as a control (NEM). Arrows indicate Tpk1 (black) and Tpk1-mPEG (red).

bioRxiv preprint doi: https://doi.org/10.1101/676270; this version posted June 30, 2019. The copyright holder for this preprint (which was not certified by peer review) is the author/funder, who has granted bioRxiv a license to display the preprint in perpetuity. It is made available under aCC-BY-NC 4.0 International license.

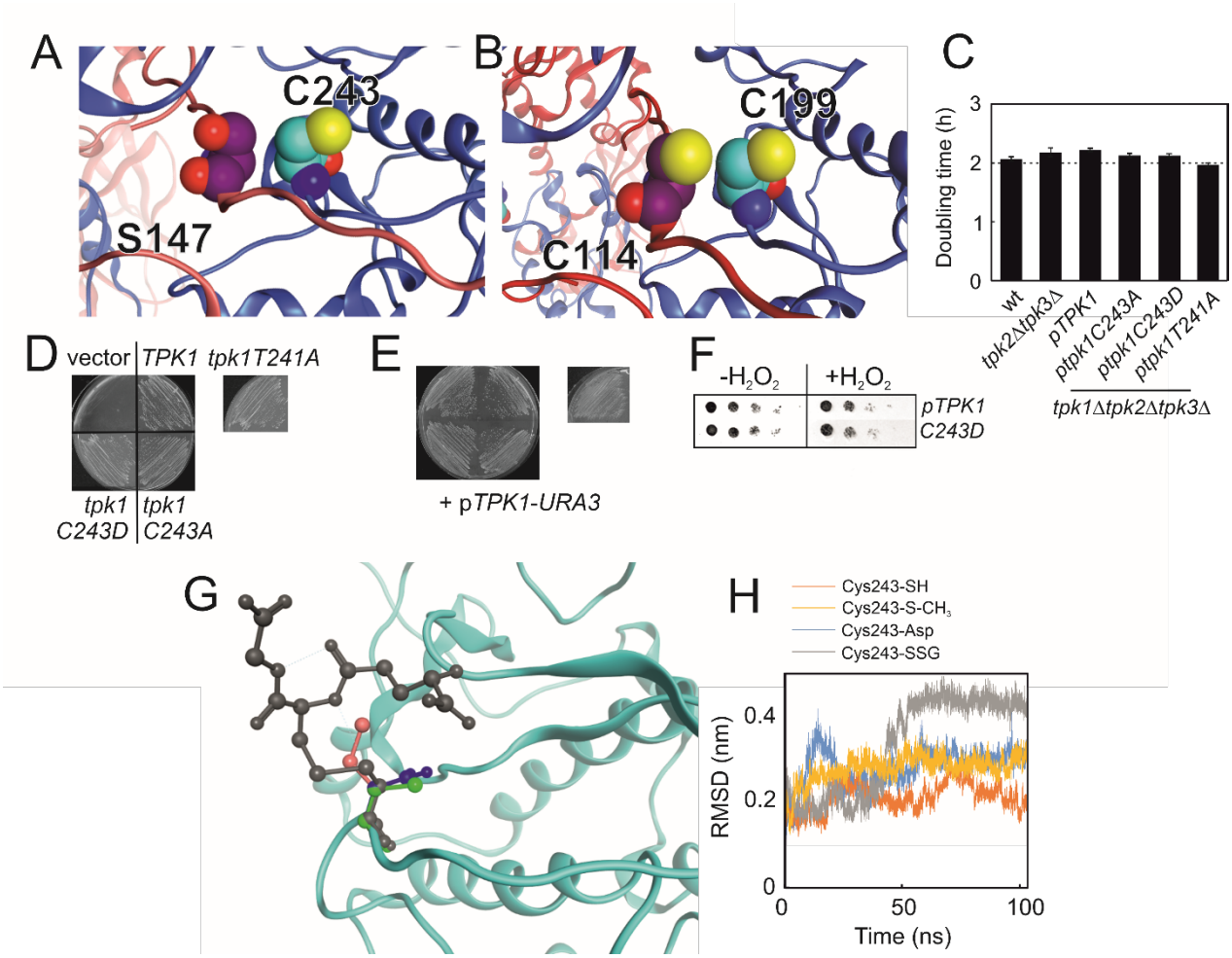

Figure S6. Related to Figure 6. Yeast PKA is redox-regulated by glutahionylation of Tpk1Cys243. **A-B)** Zoom in of the area around the conserved Cys243 in the structural homology model of the yeast holo-PKA enzyme (**A)** and Cys199 in the structure of mouse type II PKA (**B**), both comprising two catalytic subunits (C, Tpk1 in the yeast model) and two regulatory subunits (R, Bcy1 in the yeast model). **C)** Doubling time of the indicated *tpk*-mutant strains in synthetic defined -HIS medium. **D)** Growth of *tpk1Δtpk2Δtpk3Δ* cells transformed with the vector (vector) or the indicated pRS313-*TPK1* plasmids and pRS316-*TPK1* (p*TPK1-URA3*) on solid synthetic defined (-HIS, 5-FOA) medium to counterselect p*TPK1-URA3*. **E)** Growth of the strains in **D)** on solid synthetic defined selective (-HIS, URA) medium. Cells in **D)** and **E)** were left to grow for 3 days before photographed. **F)** H_2O_2 resistance of *TPK1 tpk2Δ tpk3Δ* or *tpk1C243D tpk2Δ tpk3Δ*-mutants. **G)** Alignment of cysteine (orange), aspartate (blue), methylthiolated (yellow) or glutathionylated cysteine (grey) in position 243 in the Tpk1 homology model. **H)** Root-mean-square deviation of the C-alpha distances in C243-SH (orange), Cys243Asp (blue), Cys243 methylthiolated (yellow) and C243 glutathionylated enzyme (Cys243-SSG, grey) upon molecular dynamic simulation.